DESIGN DEVELOPMENT OF THE APOLLO LUNAR MODULE*

By Kenneth J. Cox
Manned Spacecraft Center

N78-23011

ABSTRACT

The lunar module autopilot is a first-generation digital control system design. The two torque sources available for the control function of the descent-stage configuration consist of 16 reaction jets and a slow, gimbaled, throttlable engine. This case study includes a review of the design history, the design requirements, criteria, constraints, and general design philosophy of the control system development. Comparative flight-test results derived from design testing are presented.

INTRODUCTION

In the fall of 1964, a significant Apollo program decision was made; that is, to develop a digital autopilot (DAP) for all spacecraft primary control systems. It is noteworthy that previous manned spacecraft designs (Mercury, Gemini) involved analog control system techniques; thus, the Apollo DAP represents a first-generation design development. This paper contains a case study of the design history of the lunar module (LM) primary control system. The LM DAP, with respect to design requirements and constraints, is considered to be the most complex Apollo control system in use. Hence, significant original design concepts were necessarily required in the development process.

The general purpose and motivation of this paper are to provide some insight into the problems encountered by the control system designer. In many ways, the so-called "gap" between control system theory and practice is the result of a lack of appreciation of the severe/time and cost constraints under which the control system designer is required to produce his product.

Reading this paper, one may wonder why the total development has continued during a period of approximately 4 years; he may ask why the DAP should not be designed once and be finished. Most projects of this magnitude are iterative, because the requirements sometimes change radically, because the initial design constraints are generally poorly defined, because the

-1-

inherent characteristics of the spacecraft plant are not well known, and because the basic input data for control system design are frequently not available in a timely manner. It is important to realize that major design decisions must be made, rightly or wrongly, despite the lack of fundamental input information. Because of the basic factors that characteristically make the design task difficult, the designer must adopt an implicit or explicit philosophy of providing some degree of flexibility in the control design, so as to accommodate future contingencies or unexpected developmental problems.

The concept of performance margin will be examined in a later section, but a point to be recognized now is that most papers on control theory emphasize obtaining optimum (or acceptable) performance for nominal situations, whereas in practice, the acceptability of the total design is most often determined by performance under extreme, off-nominal conditions. Generally, establishing explicit mathematical criteria for off-nominal performance is extremely difficult; therefore, the subjective judgment of the system designer (who uses significant simulation testing programs for design validation) is essential.

A significant problem encountered in designing the DAP was the lack of effective analysis techniques for developing and evaluating the digital control system. The major design tools used were phase-plane simulation techniques in which tradeoffs and design constants were established by "cut-and-try" methods. A more colorful manner of expressing this approach is (1) "the [design] has been chosen on the basis of theoretical investigations and empirical observations."

LIST OF ACRONYMS AND SYMBOLS

ACRONYMS

APS	ascent propulsion system
CDU	coupling data unit
CM	command module
CSM	command and service module
DAP	digital autopilot
DB	deadband
DPS	descent propulsion system
GTS	gimbal trim system
ICS	interpretive computer simulators
IMU	inertial measurement unit
LGC	LM guidance computer
LM	lunar module
PIPA	pulsed integrating pendulous accelerometer

PRM	pulse-ratio modulation
RCS	reaction control system
SM	service module
TJET	time (duration) of jet firing

SYMBOLS

A_{os} = estimated offset angular acceleration

a,b,c = mass property parameters

B = intercept constant

CDU = coupling data unit angle

$E,\dot{E}$ = attitude and rate errors

I = I(M) pitch or roll moment of inertia

$I_{yy}I_{zz}$ = principal moments of inertia

K = filter weights

L = L(M) distance from hinge pin of descent engine bell to center of mass of LM

M = estimated mass

M_U,M_V = applied torque

$[M]$ = gimbal-to-pilot increment matrix

$\left[M_{GP}\right]$ = transformation from gimbal axes to pilot axes

$\left[M_{PC}\right]$ = transformation from pilot axes to control axes

N = noise

N_j = integer

n_t = number of sample periods

P,Q,R = pilot axes

P,U,V = control axes

T = control sample period

T_c = thrust command

t = time

u_Q,u_R = urgency functions

u = trim gimbal drive command (+1, 0, -1)

V = velocity

W = Kalman filter gains

Greek Letters

α = angular acceleration

β = lag angles

$\dot{\gamma}$ = transformation angle between U/V and U'/V' axes

ΔT_C = steering sample period

ΔT_S = control sample period

$\dot{\delta}$ = gimbal drive rate of descent engine = 0.2 deg/sec

ε = PRM attitude error

θ = gimbal angle, attitude

ω = angular velocity

Subscripts

C = cycle

cg = center of mass

d = desired angular velocity

e = attitude error

G = gimbaling

I = inner gimbal angle

i = index

J = about an axis from the firing of a single jet

M = middle gimbal angle

m = index

n = index

0 = outer gimbal angle

Operators

$\wedge$ = estimate

$\cdot$ = first time derivative

$\cdot\cdot$ = second time derivative

$\sim$ = measured value

$\sum$ = summation

DESIGN CONSIDERATIONS

Vehicle Characteristics

The DAP provides stabilization and control of the LM during both coasting and powered flight in three configurations — descent (Figure 1), ascent (Figure 2), and docked with the command and service module (CSM) as shown in Figure 3. During the preliminary spacecraft-design phase, many fundamental decisions were made that define (and constrain) the control system design. For the LM, three basic propulsion force and torque systems were established — reaction control system (RCS), descent propulsion system (DPS), and ascent propulsion system (APS). Characteristics that influenced the control task included the type of actuation system, the geometrical location and number of thrusters or jets (for redundancy), and the type of thrust-variation system.

The control options available to the systems designer are divided into various flight-mode categories (Table I). The RCS
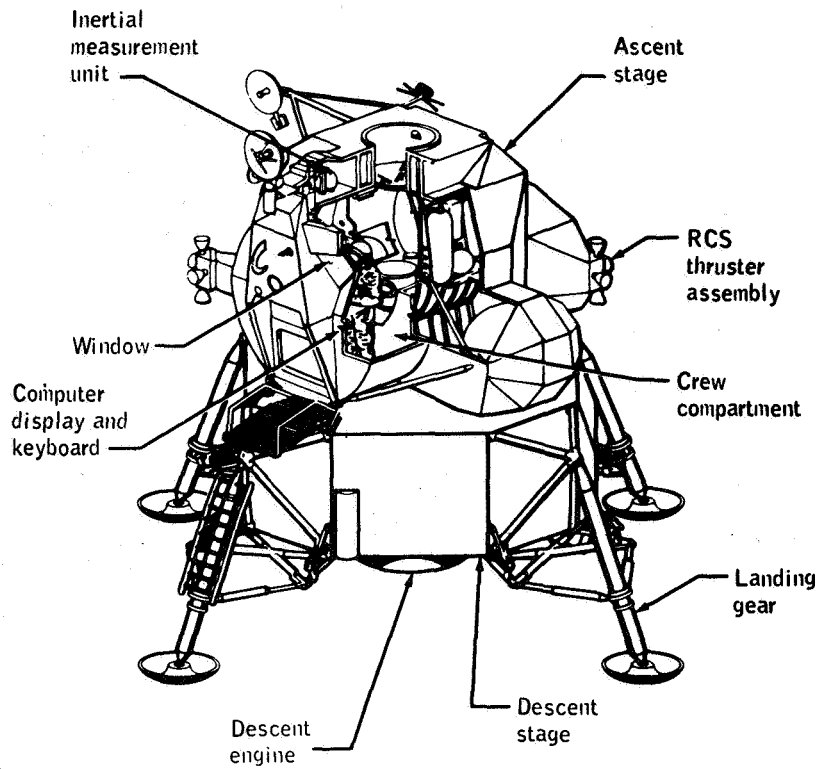
Inertial
measurement
unit

Ascent
stage

RCS
thruster
assembly

Window

Computer
display and
keyboard

Crew
compartment

Landing
gear

Descent
stage

Descent
engine

Figure 1.   The LM descent configuration
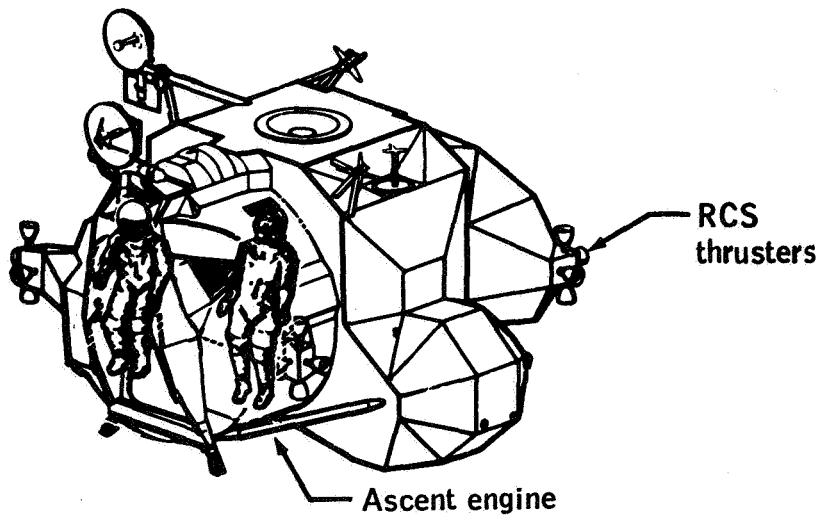
RCS
thrusters

Ascent engine
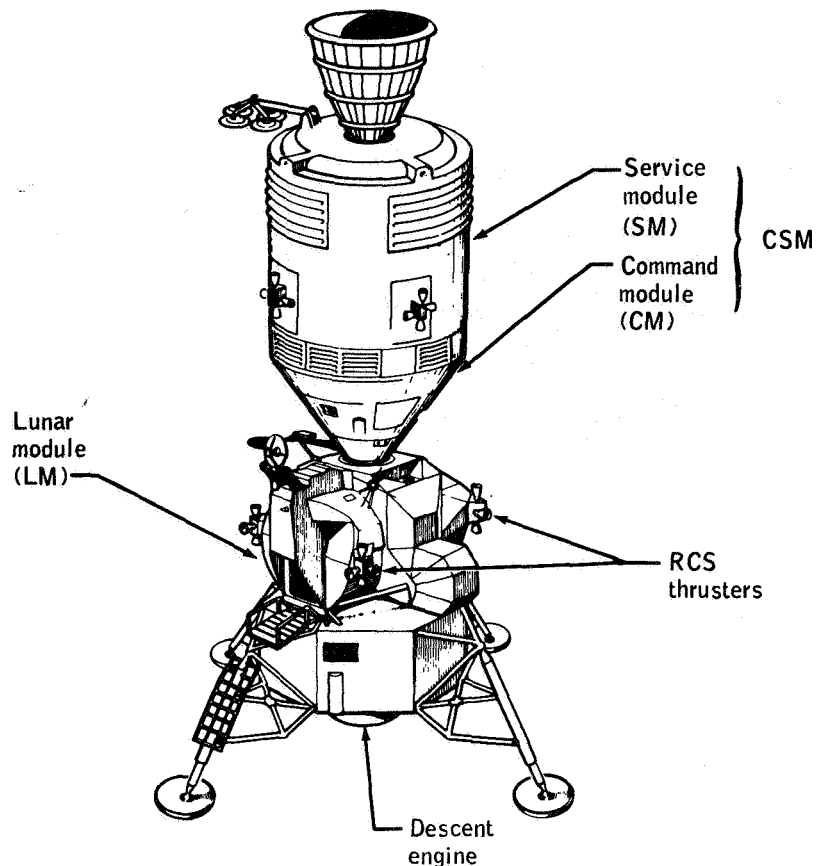
Figure 2.   The LM ascent configuration

Figure 3. The CSM-docked configuration of the LM

provides automatic/manual rotation and small translation control
for all LM configurations during coasting flight. During coasting
flight, the design problem is characterized by the presence of
extremely low disturbance torques (except for an RCS jet-on
failure).

During APS-powered flight, the primary purpose of the RCS
is to provide attitude stabilization and control. However, when-
ever feasible, it is a design requirement to fire only the
upward-thrusting RCS jets to obtain ΔV in the desired direction.
Because the APS is a non-gimbaled, fixed-throttle system, the
RCS control laws associated with this mode must accommodate large
time-variant disturbance torques.

During DPS-powered flight, the design provides yaw control
with the RCS jets, and pitch/roll attitude control with a com-
bination of the RCS and the gimbal trim system (GTS). The design

TABLE I

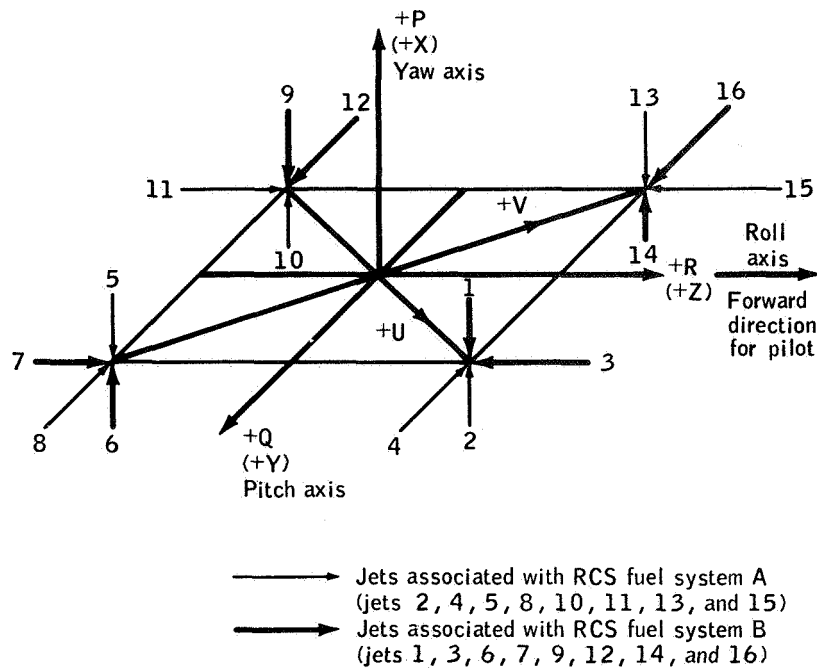CHARACTERISTICS OF SPACECRAFT PROPULSION FORCES AND MOMENTS

Propulsion force/moment	Vehicle configuration	Characteristics	Control function
Reaction control system	LM descent, LM ascent, LM/CSM	16 jets mounted in 4 quads 45 deg off Y/Z body axes centerline. Nominal force of 100 lb., arm length of 5.5 ft.	P-, U-, V-axis control for all configurations
Descent propulsion system	LM descent, LM/CSM	Throttable engine (1,050 to 10,500 lb.) with slow-speed gimbal actuators in Q-, R-axes	Q-, R-axis control for both configurations
Ascent propulsion system	LM ascent	Constant-thrust engine (3,500 lb.) fixed with respect to spacecraft	None

problems associated with dual control, including interactions between RCS and GTS modes, were significant for the DAP. As previously mentioned, the geometrical location of the RCS jets is significant in establishing the fundamental design approach. The locations of the RCS jets are shown in Figure 4. The eight X-axis RCS jets inherently provide control about the U/V axes, where the natural axes to consider phase-plane logic design are the Q/R pilot (or body) axes. The descent engine (not shown) is gimbaled about the pitch (Q) and roll (R) axes.

An important parameter not shown in Figure 4 is the distance from the spacecraft center of mass to the geometric center of the 16 RCS jets. This equivalent arm length is dependent upon both configuration and propellant loading, and strongly influences the ability to translate in the Y or Z direction.

Sensor Characteristics

The sensor information available for the control-design problem is provided by an inertial platform called the inertial

+P
(+X)
Yaw axis

9 12   13   16

11 ——————→   ————15

+V

Roll
axis

14 +R
(+Z) Forward
direction
for pilot

5

10

+U

7 ——→   ←—— 3

8 6   +Q   4   2
(+Y)
Pitch axis

———————→ Jets associated with RCS fuel system A
(jets 2, 4, 5, 8, 10, 11, 13, and 15)
———————→ Jets associated with RCS fuel system B
(jets 1, 3, 6, 7, 9, 12, 14, and 16)

Notes

1. The arrows indicate thrust direction.

2. The P, Q, and R designations for the pilot axes and the
P, U, and V designations for the control axes are used
in connection with rotation. The X, Y, and Z designation
are used in connection with translation.

Figure 4. - Locations of RCS jets on LM

measurement unit (IMU). For attitude information, gimbal angles
are provided through a coupling data unit (CDU). Basic trans-
lational information is sensed by pulsed integrating pendulous
accelerometers (PIPA's) located on the inertial platform. Early
in the design process, the decision was made to eliminate the
requirement for an independent set of rate-gyro sensors for the
control function. Thus, the attitude-state-estimation function
of the DAP is required to provide rate estimation, filtering (for
stabilization), and disturbance-acceleration estimation (when
appropriate).

Control-Mode Requirements

    The DAP control modes are established primarily by mission
requirements. The three required capabilities are for general
attitude maneuver and attitude hold, general RCS translation, and

-8-

DPS/APS-powered-flight maneuvers. A listing of the control modes associated with the present design is presented in Table II. The design of the control modes requiring phase-plane logic will be emphasized in this case study.

Design Constraints

Numerous constraints influenced the DAP design, the most predominant class of which related to weight restrictions associated with the lunar-landing program. Weight considerations constrained the system design in structural characteristics of the LM/CSM — structural bending modes are significant; in propellant-sloshing dynamics — slosh baffles were removed early in the program; and in unbalanced couple-control requirements for APS-powered flight.

TABLE II

CONTROL-MODE STRUCTURE OF THE DAP

Coasting Flight	Powered Flight
Attitude hold	Attitude hold
Automatic maneuvering	Automatic steering
Manual attitude rate	Manual attitude rate
Manual X-axis rotational override	Manual X-axis rotational override
Rotational minimum impulse	Manual translation
Manual translation	

Another class of constraints, generally identified late in the design-development phase, involved restrictions on RCS jet firing. These restrictions included duty-cycle constraints (because of propulsion instabilities), exhaust-contamination constraints (particles on windows, optics), thermal constraints (rendezvous radar, antennas, spacecraft-impingement heating), and operational constraints (during extravehicular activity docking).

A third class of constraints that influenced the design problem was associated with propulsion-system characteristics. The slow-speed trim-gimbal-actuator characteristics of the DPS were established for crew safety to avoid hardover actuator failures during powered descent of the LM. A special gear drive was developed to restrict the trim-gimbal-drive rate to ± 0.2 deg/sec. Unlike the classical actuator used for the CSM thrust-vector-control system, the DPS actuator cannot fail at a higher drive rate. A second propulsion-system constraint was associated with the decision to have a non-gimbaled APS engine. This decision imposed significant limits on allowable center-of-mass characteristics during powered ascent flight. Unfortunately, effective

control of mass-property characteristics is extremely difficult in a program such as Apollo. Another propulsion-system constraint was associated with the decision to locate the RCS jets 45 degrees from the body axes. This geometry significantly influenced the interaction between the RCS mode (U/V axes) and the GTS mode (Q/R axes) during DPS-powered flight. With respect to design and development, effective analytical techniques were virtually nonexistent for this problem.

The fourth class of constraints that impacted the design problem included computer-oriented restrictions. The LM guidance computer (LGC) is limited in both fixed and erasable memories; in addition, definite timing restrictions are placed upon the programs required to provide the control functions.

Performance and Stability Criteria

The criteria for establishing the adequacy of the DAP design are outlined in Table III, which lists functional criteria for both coasting-flight and powered-flight control modes.

TABLE III

PERFORMANCE AND STABILITY CRITERIA OF THE DAP

Control modes	
Coasting flight	Powered flight
Transient behavior — acquisition and recovery	Stability characteristics
Limit-cycle characteristics	Integrated ΔV pointing accuracy
Attitude-maneuver-rate overshoot	Attitude-transient behavior
RCS propellant comsumption	Limit-cycle characteristics
Total number of jet firings	Steady-state attitude offset
	RCS propellant consumption
	Total number of jet firings

SCOPE OF PRESENTATION

Primary emphasis will be given to reviewing the design of the LM powered-flight modes. These modes are considerably more complicated than the coasting-flight modes and provide significant insight into the design principles. The manual modes, as well as the associated displays and astronaut LGC-input functions, are beyond the scope of this case study. Other areas that are not discussed include ground/spacecraft interfaces, general operational procedures, and software-implementation techniques (including coding verification).

DESIGN PHILOSOPHY

General Design Guidelines

Various decisions made in the initial DAP control-system developmental plane established general design guidelines. A partial list of these guidelines includes:

1. Simultaneous three-axis attitude maneuvering is required (as opposed to sequential-maneuver techniques).

2. Attitude rotation shall have RCS priority logic over translation (an alternate technique is a share-type logic).

3. The control system must provide acceptable performance with single RCS jet failures (on/off), with reasonable inertia-mismatch variations, and without information about single externally disabled jets.

4. The spacecraft mass-property information must be updated during DPS/APS powered-flight maneuvers.

5. The GTS control loop must be stabilized independently of the RCS control loop.

General Philosophy

Initially, an important question with respect to design philosophy was how to use the inherent flexibility associated with a spacecraft digital computer. This question was especially significant because the DAP represented a first-generation, digital design development. Emphasis was placed upon using digital capabilities, such as logic (switching, branching), non-linear computations, and function generation. For example, design considerations of the timing structure for the RCS/GTS control laws during DPS-powered flight included consideration of simultaneous

control, sequential control, and time-interlaced logic control. These options are generally limited to analog control-system design. Another example was the reduction of switching-line chatter by logical branching to achieve improved performance under inertia mismatch, undetected jet failures, and ullage (X-axis translation) maneuvers.

The concept of performance margin was an area of design philosophy that influenced DAP development. This concept emphasized the principle that the acceptability of the design should be based upon performance of the system during extreme (but required) degraded conditions. Acceptable performance during off-nominal conditions, such as single undetected jet failures, and large control-effectiveness uncertainties (thrust magnitude, inertia properties, thrust misalignment, actuator drive rates, etc.) was difficult to achieve. The performance-margin concept identified a general trade-off between lowering the nominal to achieve acceptable performance during degraded conditions and maintaining high nominal performance despite severe degradation during off-nominal conditions. The control-system designer must use insight and judgment in establishing the degree of degradation (or margin) to which the design must accommodate in terms of performance. Even after this philosophy has been adopted, the ability to develop explicit mathematical criteria for off-nominal performance is still generally difficult to establish.

Another general philosophy was maximum utilization of modern control-theory techniques and frequency-domain techniques associated with sampled data-control systems. For example, the original attitude-state estimator developed for the DPS-powered flight was a Kalman filter. In addition, the GTS control loop was developed as a time-optimal control law. The many analytical methods available at that time were reviewed in reference 2, the authors of which implied that state phase-plane techniques (involving simulations) would probably be the primary design tools in DAP development. Techniques considered, but discarded, included convergence and stability (Liapunov, Aizeman, Lagrange), modified rate diagram, describing function, and dynamic programing. The concepts of defining regions of attraction and ultimately bounded regions were found to be inapplicable for this design development.

The philosophy of providing system-design flexibility to accommodate developmental problems or future contingencies was related to the concept of performance margin. An example was the guideline to stabilize the GTS control loop independently of RCS control loop. Three years after this design was initiated, additional thermal constraints (which essentially restricted all X-axis RCS jet firings) were identified for the LM/CSM configuration during DPS-powered flight. The design was flexible

enough to accommodate this restriction without significantly
affecting the program.

The final design philosophy listed for DAP development was
associated with the RCS propellant-performance requirements.
Design emphasis to achieve efficient propellant usage should be
placed upon those control functions that require the largest
amount of propellant over a complete mission profile. For the
DAP, these control functions included manual translations, manual
and automatic-attitude maneuvers, and maneuvers associated with
powered-flight guidance. In this general sense, the importance
of efficient RCS propellant performance for coasting-flight and
powered-flight minimum-impulse operation should be downgraded.
Thus, one may reasonably ask why design complexity (and assoc-
iated verification) should be increased to save 20 percent per-
formance on an item that uses 5 percent of the total mission pro-
pellant. A definite trade-off exists between design complexity
and performance-improvement payoff.

DESCRIPTION OF DAP DESIGN

The DAP design that was flight-tested on the Apollo 9 manned
mission will be described in this section. This design (assoc-
iated with the SUNDANCE flight ropes) is described in reference 3,
and will be treated as the base line design for the case study.
Virtually all of the following design descriptions are condensed
from reference 3.

Coasting-Flight Modes

The two coasting-flight modes described are the attitude-
hold mode, and the automatic-maneuver mode. A block diagram of
the coasting-flight attitude-hold mode is presented in Figure 5.

The major design elements include the attitude-state estimator,
the RCS control laws, and the jet-selection logic, functional
descriptions of which are provided in this section.

The basic measurements available to the recursive state
estimator are the three gimbal angles from the IMU. The estimator
for coasting flight predicts both attitude and angular velocity,
and uses non-linear threshold logic to reject low-level measurement
noise. Angular-acceleration information caused by RCS jet firings
is an additional input to the state estimator.

The RCS control laws compute the requirements for rotational
impulses, using information based upon attitude phase-plane errors,
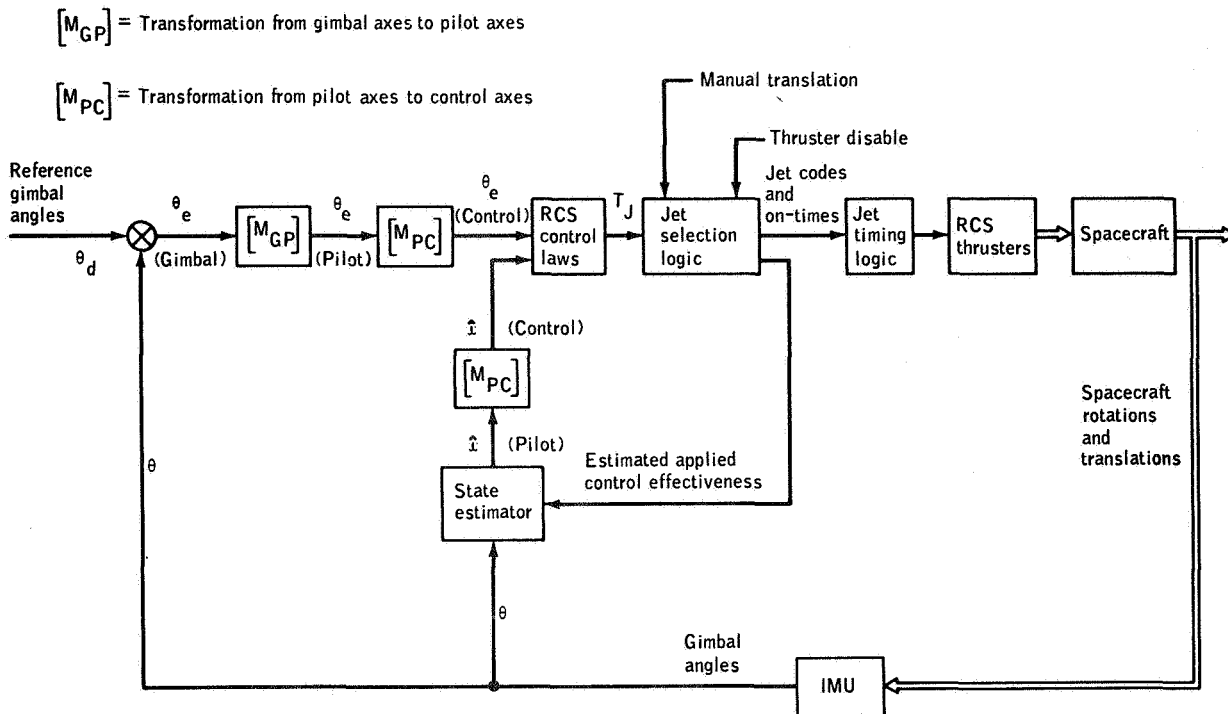control effectiveness, and phase-plane targeting logic.

$\left[M_{GP}\right]$ = Transformation from gimbal axes to pilot axes

$\left[M_{PC}\right]$ = Transformation from pilot axes to control axes

Reference gimbal angles

Manual translation

Thruster disable

θ_e (Gimbal) $\quad$ $\left[M_{GP}\right]$ $\quad$ θ_e (Pilot) $\quad$ $\left[M_{PC}\right]$ $\quad$ θ_e (Control) $\quad$ RCS control laws $\quad$ T_J $\quad$ Jet selection logic $\quad$ Jet codes and on-times $\quad$ Jet timing logic $\quad$ RCS thrusters $\quad$ Spacecraft

θ_d

$\hat{x}$ (Control)

$\left[M_{PC}\right]$

$\hat{x}$ (Pilot)

Estimated applied control effectiveness

Spacecraft rotations and translations

State estimator

θ

θ

Gimbal angles

IMU

Figure 5. – Coasting-flight attitude-hold mode

The jet-selection logic combines the required rotational impulses with the commanded translation inputs to select appropriate jets for control action. Additional information used by the jet-selection logic includes the desired number of jets to be fired and the identification of disabled jets.

Additional design elements shown in Figure 5 are transformation equations and jet-timing logic. The transformation equations, from gimbal to pilot axes, and from pilot to control axes, are straight-forward, not to be presented explicitly. The jet-timing logic is used to establish mandatory conditions for two-jet control in the U/V axes, and for four-jet control in the P-axis.

A block diagram of the coasting-flight automatic-maneuver control mode is presented in Figure 6. Automatic maneuvers are implemented using the same logic as attitude hold, except for the attitude-maneuver routine. This routine provides desired steering commands in both attitude and rate, as well as generating a set of lag angles β. These lag angles are introduced to prevent overshoot when initiating or terminating an automatic maneuver. The simplified single-plane equations for the attitude-maneuver routine are given as

-14-

$$\Delta\theta_d(t_n) = \left[\theta_d(t_n + 1) - \theta_d(t_n)\right]\frac{\Delta T_S}{\Delta T_C} \tag{1}$$

$$\theta_d(N_j) = \theta_d(N_{j-1}) + \Delta\theta_d(t_n) \tag{2}$$

$$\beta = \frac{\omega_d|\omega_d|}{2\alpha_J} \tag{3}$$

where Equation (1) is computed every steering cycle ($\Delta T_C = N_j - N_{j-1} = 2$ sec), and Equation (2) is computed every control cycle ($\Delta T_S = 0.1$ sec). The value of ω_d is set by the maneuver-rate input, and α_J is defined as the magnitude of the assumed two-jet acceleration. When the maneuver is completed, ω_d, $\Delta\theta_d$, and β are reset to zero, and the control system reverts to attitude hold about the desired gimbal angles.

Powered-Flight Automatic Mode

The control operations associated with powered flight are considerably more complicated than coasting-flight operations. Major additions for both DPS- and APS-powered flight include an integrated guidance and navigation outer loop that interfaces with the DAP through a steering routine, and a mass monitor-and-control parameter routine. In addition, the state estimator is required to derive offset angular acceleration α. The RCS control laws are modified by making the control effectiveness and the phase-plane targeting logic dependent upon the estimated offset angular acceleration. During DPS-powered flight, a control law for the GTS is required. A timing-and-control-logic interaction between the RCS control and the GTS control is also required. A block diagram of the APS powered-flight automatic control is presented in Figure 7. The major design elements (state estimator, control laws, jet-selection logic) will be discussed in detail in the following sections.

Control Effectiveness

The DAP control laws and the recursive state estimator require information on the assumed RCS and GTS control effectiveness. The GTS control effectiveness is represented by the rate of change of angular acceleration, $\dot{\alpha}_G$, caused by constant angular-drive-rate command to the actuators. A flow diagram indicating those factors that relate to the GTS control effectiveness is presented in Figure 8. The factors indicated in Figure 8 are as follows:

M   = estimated mass
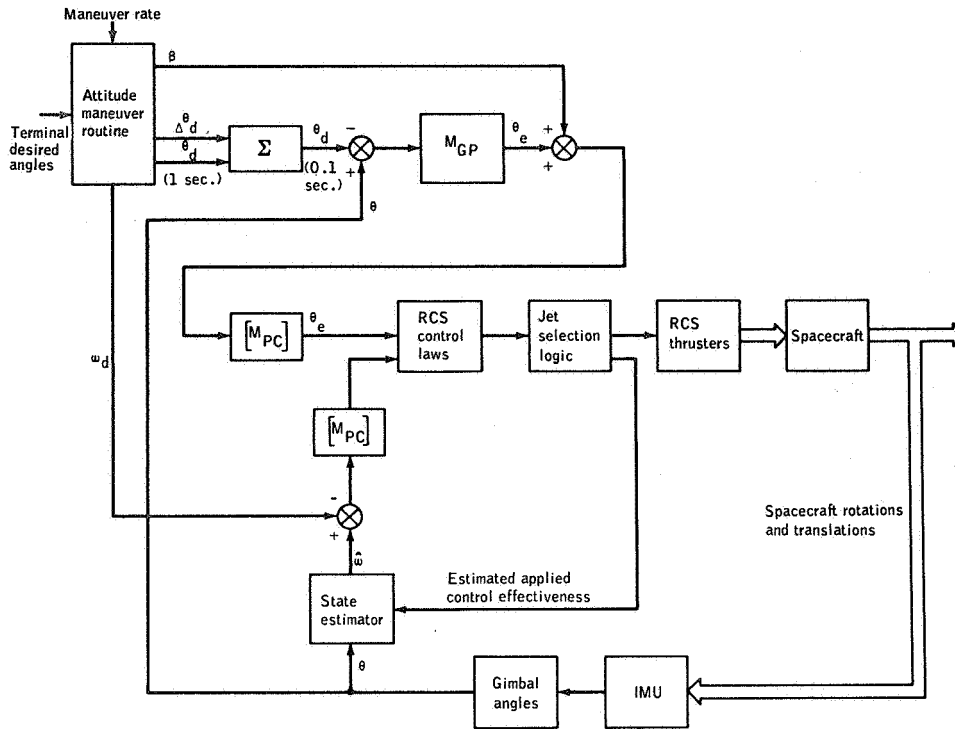L   = L(M) distance from hinge pin of descent engine bell to center of mass of LM
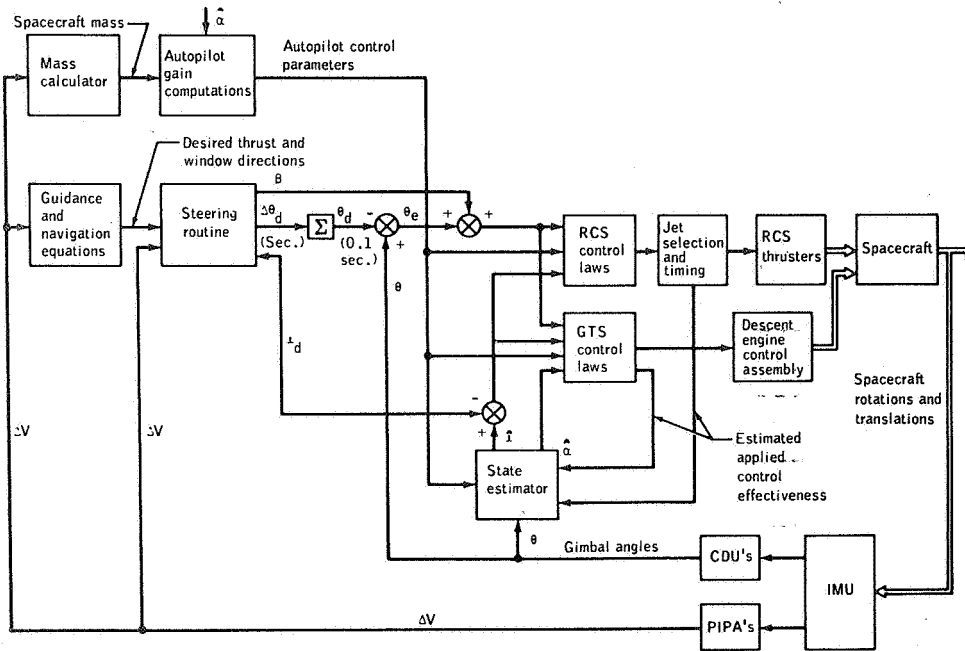
-15-

Figure 6. - Coasting-flight automatic-maneuver mode

Figure 7. - Powered-flight automatic control of the DPS

```
I         = I(M) pitch or roll moment of inertia
ΔV/Δt     = measured linear acceleration
u_Q,u_R   = trim-gimbal drive commands (+1, 0, -1)
            for Q and R channels
δ̇         = gimbal-drive rate of descent engine =
            0.2 deg /sec
```

The effectiveness of the RCS control is represented by the angular acceleration α_J about an axis from the firing of a single jet. A flow diagram containing the RCS control effectiveness equation in the P-, Q-, R-axes, and the appropriate equations for transformation to the P-, U-, V-axes is presented in Figure 9. To represent the RCS angular acceleration as a hyperbolic function of mass, a nominal jet-torque level of 550 foot-pounds is assumed, and additional vehicle configuration assumptions are required to establish inertia characteristics as a function of mass.

State Estimator

The recursive state estimator for powered and coasting flight is described in this section. The most complex estimator design, associated with DPS-powered flight, will be described first. Kalman filter theory provides a reasonable structure for combining estimates of state changes caused by RCS jet firings and trim-gimbal activity with external measurements of attitude. The LM plant is assumed to be represented by a simplified set of rigid body equations of motion

$$\dot{\theta} = \omega \tag{4}$$

$$\dot{\omega} = \alpha + U_J \tag{5}$$

$$\dot{\alpha} = U_G + N_{cg} \tag{6}$$

where θ   = attitude
      ω   = angular velocity
      α   = offset angular acceleration caused by
            DPS/APS thrust
      U_J = angular acceleration caused by RCS jet
            firings
      U_G = rate of change of angular acceleration
            caused by descent engine gimbaling
      N_{cg} = rate of change of angular acceleration
            caused by center-of-mass movement

The time histories of the control outputs U_J and U_G between sample instant t_{n-1} and t_n are assumed to be the values commanded, and are represented by
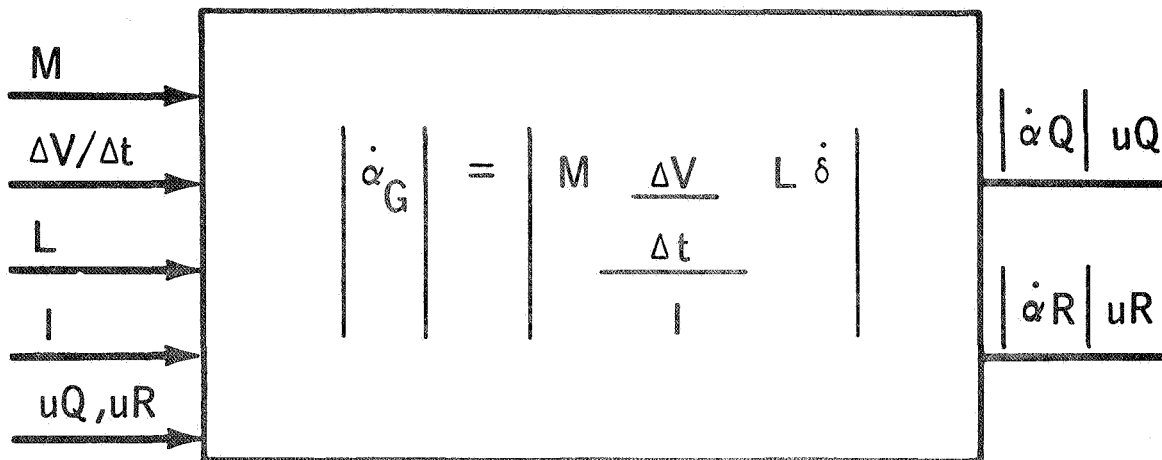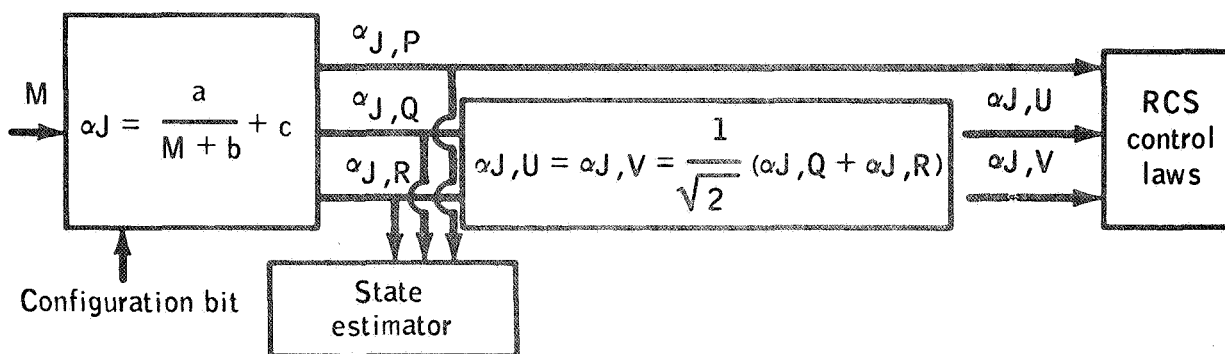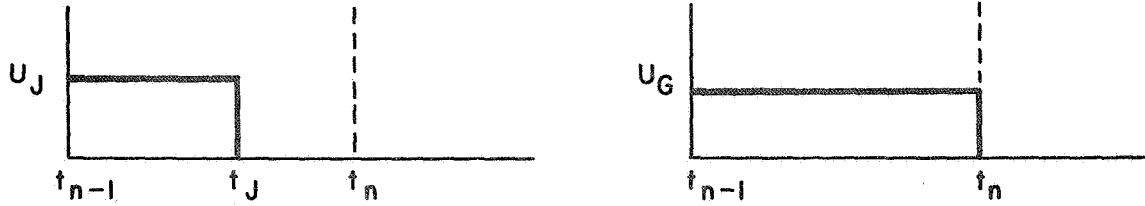
Figure 8. - Control effectiveness of the GTS

Figure 9. - Control effectiveness of the RCS

-18-

where $T = t_n - t_{n-1}$ = control-sample period.

The measurement equation is expressed by

$$\theta_m = \theta + N \tag{7}$$

where N = measurement noise from vibration, tracking errors of the CDU, and quantization. The estimation process requires the development of equations for state extrapolation and measurement incorporation. Given the estimate of the state $\hat{\theta}$, $\hat{\omega}$, $\hat{\alpha}$ at t_{n-1}, and assuming the time histories of U_J and U_G between t_{n-1} and t_n, the extrapolated state at t_n is obtained by integrating Equations (4), (5), and (6) to obtain

$$\theta'\left(t_n\right) = \hat{\theta}\left(t_{n-1}\right) + \hat{\omega}\left(t_{n-1}\right) T + \hat{\alpha}\left(t_{n-1}\right)\frac{T^2}{2}$$
$$+ U_G \frac{T^3}{6} + U_J t_J \left(T - \frac{t_J}{2}\right) \tag{8}$$

$$\omega'\left(t_n\right) = \hat{\omega}\left(t_{n-1}\right) + \hat{\alpha}\left(t_{n-1}\right) T + U_G \frac{T^2}{2} + U_J t_J \tag{9}$$

$$\alpha'\left(t_n\right) = \hat{\alpha}\left(t_{n-1}\right) + U_G T \tag{10}$$

The extrapolated attitude variables are compared with the external measurements to obtain an updated estimate at t_n

$$\hat{\theta}\left(t_n\right) = \theta'\left(t_n\right) + K\theta\left[\theta_m\left(t_n\right) - \theta'\left(t_n\right)\right] \tag{11}$$

$$\hat{\omega}\left(t_n\right) = \omega'\left(t_n\right) + \frac{K\omega}{T}\left[\theta_m\left(t_n\right) - \theta'\left(t_n\right)\right] \tag{12}$$

$$\hat{\alpha}\left(t_n\right) = \alpha'\left(t_n\right) + \frac{K\alpha}{T^2}\left[\theta_m\left(t_n\right) - \theta'\left(t_n\right)\right] \tag{13}$$

If the filter weights, K_θ, K_ω, and K_α, are optimized based upon Kalman filter theory, the values are time variant, and are

dependent upon the values of N_{cg} and N, and the uncertainty in the initial state estimate. During the design development of the DAP, the optimum filter-gain concept was discarded after many problems were identified through simulation testing. At that time, a nonlinear threshold filter was developed as part of the base line design. This filter and the threshold values assoc- iated with the concept were established from direct engineering considerations.

Development of the nonlinear threshold filter was motivated by the specific properties of the measurement noise from the IMU. For the design considered, the predominant measurement noise is derived from the nonlinear-tracking servo characteristics of the electronic CDU's. Gimbal-angle information encoded in the LGC (for moderate angular vehicle velocities) contains high-frequency noise having a peak-to-peak amplitude of approximately 0.09 degree. It is important to note that the distribution of this noise is rectangular rather than gaussian. A trap filter using threshold logic was developed to reject this type of low-level measurement noise. The logic and associated filter-gain equations are as follows. If $|\theta_m - \theta'| \leq \theta_{max}$, then

$$K_\theta = K_\omega = K_\alpha = 0 \tag{14}$$

If $|\theta_m - \theta'| > \theta_{max}$, then

$$K_\theta = 1$$

$$K_\omega = \frac{1}{n_t + N_\omega}$$

$$K_\alpha = \frac{1}{n_t + N_\omega + N_\alpha} K_\omega \tag{15}$$

where θ_{max} = threshold value (0.14 degree)
N_ω = rate gain constant
N_α = acceleration gain constant
n_t = number of sample periods that have elapsed since the threshold was exceeded last

Extensive testing has demonstrated that the nonlinear thres- hold logic successfully rejects low-level measurement noise. This filter also performs well with respect to disturbances that are cyclic in nature, such as slosh and structural vibrations. The filter gains for the rate and acceleration estimates derived by

Equation (15) are functions of n_t. If the trap overflows almost every time, it is generally desirable for the filter characteristics to provide a fast rate estimate and a slow acceleration estimate. The desired response time on the acceleration estimate is set by requirements to track a moving center of mass and to respond to time-variant thrust-actuation compliance effects. The upper limit on response time is restricted because of the desire to avoid rapid fluctuations in the autopilot switching curves and because of the requirement to attenuate slosh accelerations.

If the threshold logic be exceeded only rarely, a maximum incorporation of the measurement is generally desired. The logic given in Equations (14) and (15) is actually a simplification of the developed design. The threshold value is actually compared with the total unexplained attitude that has accumulated since the last trap overflow, where the incremental amount for one control-sample period is the difference between the measured and the predicted changes in attitude.

A summary of the input and output variables associated with the state estimator for DPS-powered flight is presented in Figure 10.

The structure of the estimator for APS-powered flight is identical except that the variables associated with the GTS are deleted. Similarly, the state estimator for coasting flight is based upon the same structure, except that the estimated state does not include offset angular acceleration. The total estimator design represents an integrated concept with respect to both powered and unpowered modes of control. To conclude this section, the dynamical effects not explicitly considered in th initial development of the filter equations will be iden fied, as follows:

1. Propellant-slosh dynamics

2. Structural-bending dynamics

3. Jet-impingement-forces model

4. Jet-thrust lags

5. Jet-misalignment geometry

6. Jet acceleration caused by Y/Z translation

7. Undetected jet failures

8. Trim-gimbal lags

9. Inertial mismatch

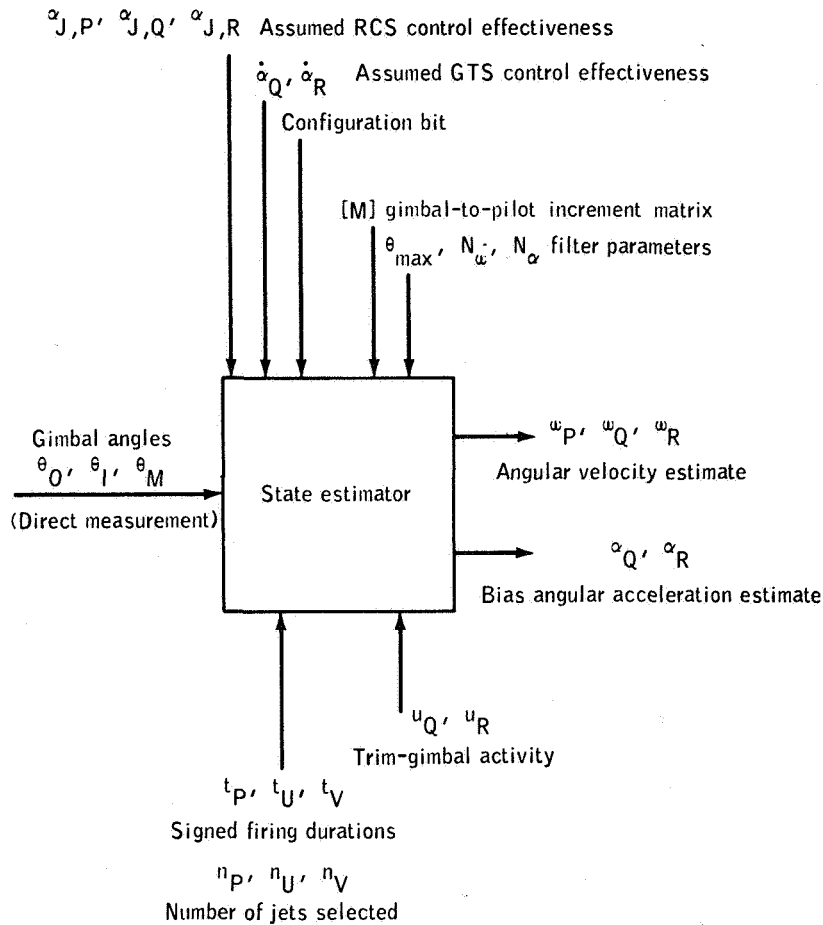10. DPS-actuator-compliance model

11. Propellant-fuel-shift model

$\alpha_{J,P}$, $\alpha_{J,Q}$, $\alpha_{J,R}$ Assumed RCS control effectiveness

$\dot\alpha_Q$, $\dot\alpha_R$ Assumed GTS control effectiveness

Configuration bit

[M] gimbal-to-pilot increment matrix

θ_{max}, $N_{\dot\omega}$, N_α filter parameters

Gimbal angles

θ_O, θ_I, θ_M

(Direct measurement)

State estimator

ω_P, ω_Q, ω_R

Angular velocity estimate

α_Q, α_R

Bias angular acceleration estimate

u_Q, u_R

Trim-gimbal activity

t_P, t_U, t_V

Signed firing durations

n_P, n_U, n_V

Number of jets selected

Figure 10. - Input and output variables of the state estimator

Other assumptions that modified the estimator equations implemented in the filter design were that the cross products of inertia terms were ignored; that the terms in Equations (8) and (9) caused by the trim-gimbal drive U_G were deleted; and that second-order rate terms were ignored in the equations of motion.

Detailed verification testing was required to demonstrate the stability and performance, including the known dynamical effects, of the total system. Simulation testing supported the establishment of the critical filter values of θ_{max}, N_ω, and N_α.

An important consideration was testing the filter performance when an undetected jet-off failure existed. When this condition occurs, the acceleration estimate will seek an average value double the actual acceleration offset present. Because the DPS acceleration-nulling control law is a function of the sign of the acceleration-offset estimate, and is invariant with the magnitude, this control law will seek the center of mass properly when undetected jet-off conditions exist.

RCS Control Laws

The control laws associated with the RCS establish jet-firing durations (TJET values) based upon phase-plane logic and assumed control effectiveness. These control laws are predictive in nature and are related to the classical two-point-boundary-value problem. To some extent, this predictive design is inherently sensitive to the uncertainties in control effectiveness and unmodeled disturbances. A description of the TJET LAWS associated with the LM descent and ascent configurations is provided in this section.

Angular error/error-rate phase planes are established for each P, U, and V RCS control axis. Because the sets of jets that produce rotation about each of these three axes are distinct, the P-, U-, and V-axis jets are turned on and off independently. A block diagram of the control-law inputs for the LM descent and ascent configurations is presented in Figure 11.
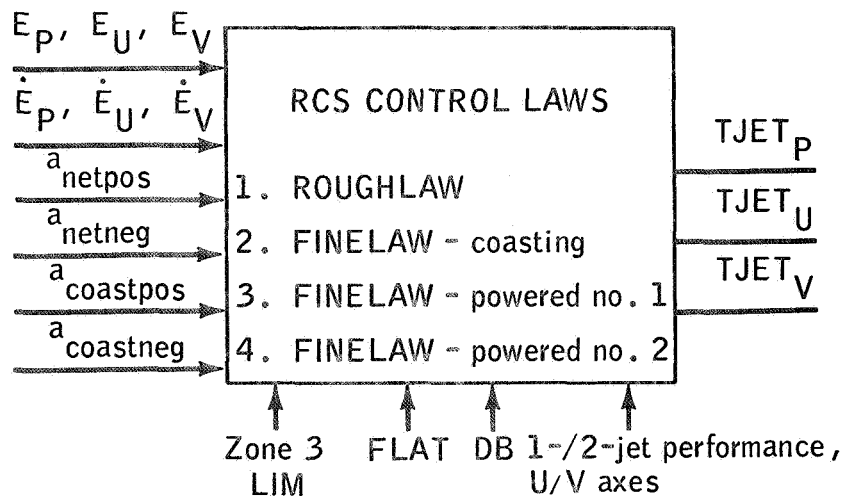
Figure 11. — TJET LAWS, LM only

The attitude and rate errors $(E, \dot{E})$ are used to establish the estimated state location in the phase plane. The acceleration inputs required by the RCS control laws include net angular acceleration (jet acceleration plus offset acceleration), and

-23-

coasting acceleration (acceleration caused by offset alone). The
basic shape of the target parabolas and switching-line parabolas
are set by this angular-acceleration information. Additional
inputs — deadband (DB) and FLAT — establish the positional loc-
ation of these parabolas. The four different phase-plane config-
urations associated with the DAP design are listed in Figure 11.
The TJET control logic is developed by dividing each phase-plane
configuration into coasting and firing zones.

The ROUGHLAW phase-plane configuration shown in Figure 12
is used for all control modes whenever either the magnitude of
E exceeds 11.25 degrees or the magnitude of $\dot{E}$ exceeds 5.625
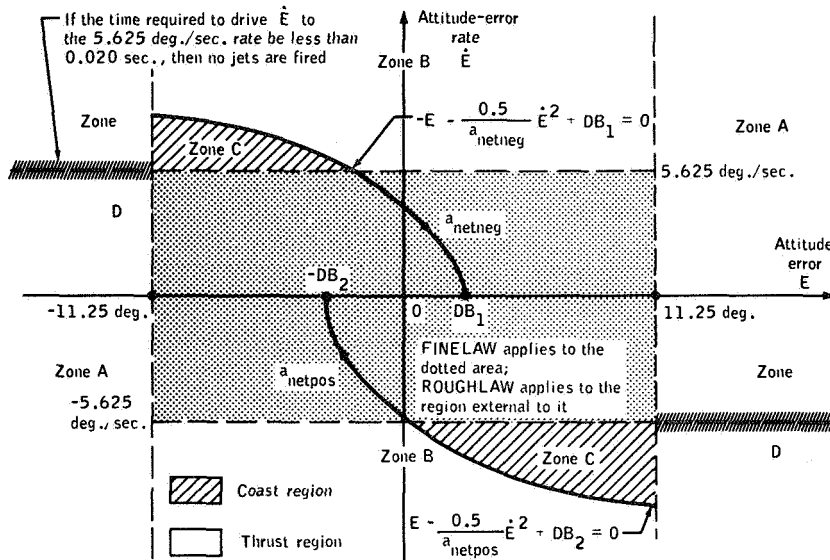
Figure 12. - The ROUGHLAW phase plane

deg/sec. If neither of these limits be exceeded, a FINELAW
phase-plane configuration is used in the RCS control logic.
The use of ROUGHLAW for large values of E and $\dot{E}$ permits the
efficient use of single precision arithmetic by the LGC. The com-
putational ability to provide independent scaling for different
regions of the error phase plane provides a significant flexibility
compared with most of the analog control-system designs. The
ROUGHLAW phase-plane configuration is divided into zones A to D.
The logic for computing TJET for the upper half plane of ROUGHLAW
is presented in Table IV.

The three phase-plane configurations associated with FINELAW
are shown in Figures 13, 14, and 15. The configurations include
drifting flight, powered-descent flight when the trim-gimbal
nulling times are less than 2 seconds, and powered-ascent flight

TABLE IV

ROUGHLAW TJET LOGIC

Location of the LM state	Basic of computing TJET
Zone A	TJET is the time required to drive $\dot{E}$ to -5.625 deg /sec.
Zone B	TJET is set equal to 0.250 sec; that is, a "large" value.
Zone C	TJET is set equal to zero, that is, no jets are turned on.
Zone D	TJET is the time required to drive $\dot{E}$ to +5.625 deg /sec.

or when the trim-gimbal nulling times are greater than 2 seconds. The FINELAW TJET logic for coasting flight is presented in Table V.

The zones 2 and 3 logic was developed to acquire a minimum-impulse limit cycle efficiently. The motivation for occasionally permitting the jets to remain on in zone 4 was to avoid switching-line chatter when the net angular acceleration is underestimated because of inertia mismatch.

The FINELAW phase-plane logic for powered-descent flight when the trim-gimbal nulling times are less than 2 seconds is identical to the coasting logic of Table V, except that zone 3 has been eliminated. This logic provides an efficient interface between the RCS and GTS control systems.

The FINELAW logic for the phase-plane configuration assoc-iated with Figure 15 is also similar to the coasting logic of Table V. The principal exceptions are that zones 2 and 3 have been eliminated, and that the logic developed from zone 4 is to target to intersect a parabola instead of the E-axis plane.

As mentioned previously, the DB_1 through DB_4 parameters, together with FLAT, are used to establish the positions of the phase-plane parabolas. The intercept values were established empirically through simulation testing, and are proportional to the DB. The proportionality constants, which were developed to depend logically upon the estimated offset acceleration, are
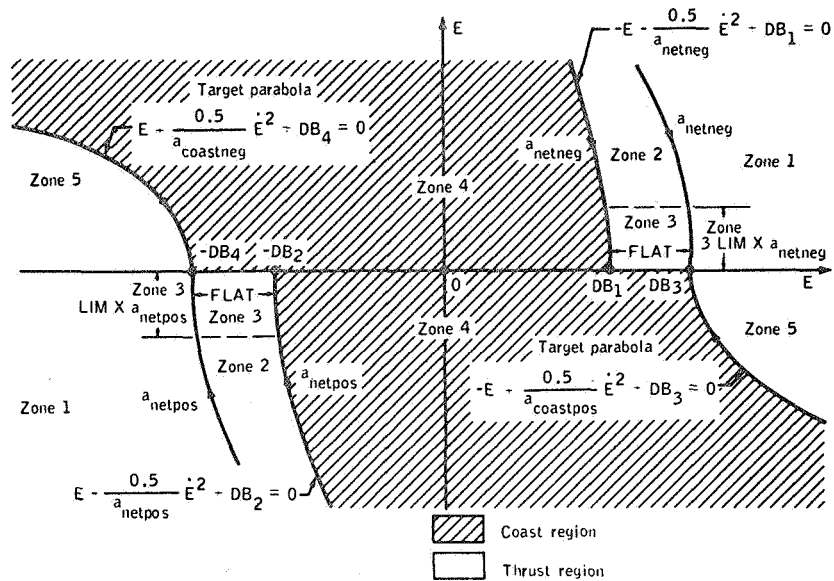
Figure 13. - The FINELAW phase plane when the LM is in
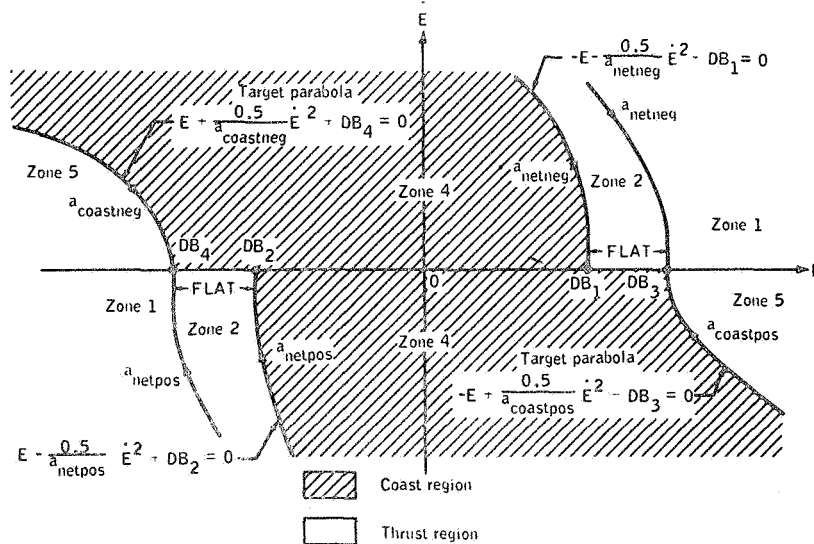drifting flight

Figure 14. - The FINELAW phase plane when both command
trim-gimbal nulling drive times are less than 2
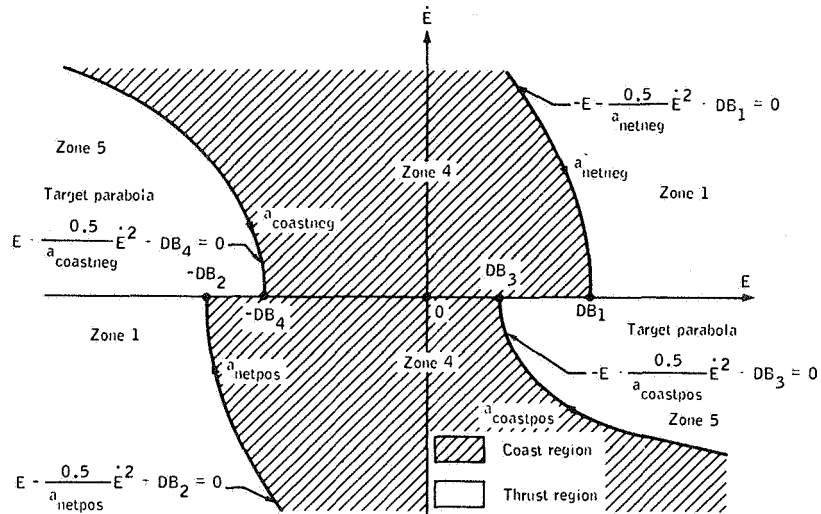seconds during powered descent

Figure 15. - The FINELAW phase plane when the LM is in powered ascent or when either of the trim-gimbal nulling drive times is greater than 2 seconds during powered descent

TABLE V

FINELAW, COASTING TJET LOGIC

Location of the LM state	Basis of computing TJET
Zone 1	TJET is the time required to drive the LM state to a "target parabola."
Zone 2	TJET is the time required to drive the LM error rate to zero.
Zone 3	TJET is set so small that the jet-selection logic will fire a one-jet minimum impulse.
Zone 4	TJET is set to zero unless the jets for the axis concerned are already on and are driving the LM state to intersect the E axis between $-DB_2$ and DB_1.
Zone 5	TJET is the time required to drive the LM state to a "target parabola."

presented in Table VI. The general design strategy was to set the position of the parabolas to yield small, average, steady-state attitude errors during powered flight. The classic analog control-system trade-off of establishing a single switching-line logic to provide adequate performance during both high- and low-disturbance-torque conditions is avoided in this design.

Another input required for the RCS control laws is the indication of one-jet or two-jet couple preference for U/V axes control. Normally, one-jet control is desired for powered ascent and X-axis translation. However, additional logic associated with large phase-plane errors is used, requiring mandatory two-jet couple control when certain conditions are exceeded.

For the P-axis, the computation of TJET is always made on the basis of two-jet couples. However, the TJET logic is over-ridden and four jets are fired for 0.1 second if certain TJET values and error-state conditions are exceeded.

Jet-Selection Logic

The RCS control laws establish requirements for some number of jets to be fired about the P-, U-, and V-axes. The translation-acceleration requirements are obtained directly from guidance inputs or manual commands. The jet-selection logic determines the RCS jet policy when provided the desired rotational torque information, the desired direction of translation, and the desired number of jets to be used for each maneuver. In addition, the firing logic is modified when jets are known to be disabled.

The jet-selection policies associated with the P-axis rotation and the Y- and Z-axis translations are presented first. Because rotation takes priority over translation, the Y- and Z-axis commands are executed only when no P-axis commands are present. The normal P-axis jet-selection policy is presented in Table VII.

If any of the rotation policies given in Table VII involves a disabled jet, then alternate two-jet rotation policies will be attempted in the following sequential order until a policy involving only enabled jets is found.

+P Rotation	-P Rotation
7, 15	8, 16
4, 12	3, 11
4, 7	8, 11
7, 12	11, 16
12, 15	3, 16
4, 15	3, 8

TABLE VI

CRITERIA TO DETERMINE THE INTERCEPT

OF THE PHASE-PLANE PARABOLAS

Define

$$a_{min} = 1.4 \text{ deg /sec}^2$$

A_{os} = estimated offset angular acceleration

For powered flight (except when both of the commanded trim-gimbal nulling drive times are less than 2 sec during powered descent)

FLAT = 0 and

a) If $A_{os} > a_{min}$,

$DB_1 = DB, DB_2 = 2DB, DB_3 =$

$-0.75DB, DB_4 = 2DB$

b) If $A_{os} < -a_{min}$,

$DB_1 = 2DB, DB_2 = DB, DB_3 =$

$2DB, DB_4 = -0.75DB$

c) If $a_{min} > A_{os} > 0.5a_{min}$,

$DB_1 = DB, DB_2 = DB, DB_3 =$

$0.5DB, DB_4 = DB$

d) If $-0.5a_{min} > A_{os} > -a_{min}$,

$DB_1 = DB, DB_2 = DB, DB_3 =$

$DB, DB_4 = 0.5DB$

e) If $0.5a_{min} > A_{os} > -0.5a_{min}$,

$DB_1 = DB_2 = DB_3 = DB_4 = DB$

For drifting flight (and when both of the commanded trim-gimbal nulling drive times are less than 2 sec during powered descent)

$$DB_1 = DB_2 = DB, DB_4 = DB_3 = DB + FLAT,$$

and FLAT = 0.8 deg

TABLE VII

P-AXIS NORMAL JET-SELECTION POLICY

Type of rotation	Jet-selection policy
4-jet, +P	4, 7, 12, 15
2-jet, +P	Alternate pulses between 4 and 12, and between 7 and 15
4-jet, -P	3, 8, 11, 16
2-jet, -P	Alternate pulses between 3 and 11, and between 8 and 16

The normal Y- and Z-axis translation policies, with alternate policies for disabled jets, are presented in Table VIII.

The jet-selection policies associated with the U- and V-axis rotations and the X-axis translation are now presented. If no conflict exists between jets required for translation and rotation, then both policies are executed. However, if a conflict exists, only the rotation policy is applied.

The U- and V-axis rotational policies for both normal and disabled-jet conditions are presented in Table IX.

Finally, the X-axis translational policies for both normal and disabled-jet conditions are presented in Table X.

If no alternate disabled-jet policies be possible, a computer program alarm is lighted and an alarm code informs the astronauts that a rotation or translation failure exists. This alarm procedure is applicable for all of the jet-selection policies presented.

GTS Control Laws

Two slow-speed actuators are used to gimbal the descent engine about the Q- and R-axes. The control modes developed for commanding these trim actuators are an attitude-control mode, and an acceleration-nulling mode.

The control law associated with the attitude-control mode has been developed to be a function of errors in attitude, rate,

TABLE VIII

Y- AND Z-AXIS JET-SELECTION POLICIES

Type of translation	Normal policy	Alternate disabled-jet policy
+Y	12, 16	If 16 has been disabled, set up the tacking policy of alternating between 12 and 3, and between 12 and 11. If 12 has been disabled, set up the tacking policy of alternating between 16 and 15, and between 16 and 7.
-Y	4, 8	If 8 has been disabled, set up the tacking policy of alternating between 4 and 3, and between 4 and 11. If 4 has been disabled, set up the tacking policy of alternating between 8 and 7, and between 8 and 15.
+Z	7, 11	If 11 has been disabled, set up the tacking policy of alternating between 7 and 8, and between 7 and 16. If 7 has been disabled, set up the tacking policy of alternating between 11 and 12, and between 11 and 4.
-Z	3, 15	If 15 has been disabled, set up the tacking policy of alternating between 3 and 4, and between 3 and 12. If 3 has been disabled, set up the tacking policy of alternating between 15 and 8, and between 15 and 16.

TABLE VIII

Y- AND Z-AXIS JET-SELECTION POLICIES (cont)

Type of translation	Normal policy	Alternate disabled-jet policy
+Z,+Y (+U)	7, 11, 12, 16	If either 11 or 12 has been disabled, use 7 or 16. If either 7 or 16 has been disabled, use 11 or 12.
-Z,-Y (-U)	3, 4, 8, 15	If either 8 or 15 has been disabled, use 3 or 4. If either 3 or 4 has been disabled, use 8 or 15.
+Z,-Y (+V)	4, 7, 8, 11	If either 4 or 11 has been disabled, use 7 or 8. If either 7 or 8 has been disabled, use 4 or 11.
-Z,+Y (-V)	3, 12, 15, 16	If either 15 or 16 has been disabled, use 3 or 12. If either 3 or 12 has been disabled, use 15 or 16.

TABLE IX

U- AND V-AXIS JET-SELECTION POLICIES

Type of rotation	Translational sense required	Normal policy	Alternate disabled-jet policy
2-jet,+U	-	5, 14	If 14 has been disabled, use 5 alone; if 5 has been disabled, use 14 alone.
1-jet,+U	+X	14	If 14 has been disabled, use 5.
1-jet,+U	-X	5	If 5 has been disabled, use 14.

TABLE IX

U- AND V-AXIS JET-SELECTION POLICIES (cont)

Type of rotation	Translational sense required	Normal policy	Alternate disabled-jet policy
2-jet,-U	-	6, 13	If 13 has been disabled, use 6 alone; if 6 has been disabled, use 13 alone.
1-jet,-U	+X	6	If 6 has been disabled, use 13.
1-jet,-U	-X	13	If 13 has been disabled, use 6.
2-jet,+V	-	1, 10	If 10 has been disabled, use 1 alone; if 1 has been disabled, use 10 alone.
1-jet,+V	+X	10	If 10 has been disabled, use 1.
1-jet,+V	-X	1	If 1 has been disabled, use 10.
2-jet,-V	-	2, 9	If 9 has been disabled, use 2 alone; if 2 has been disabled, use 9 alone.
1-jet,-V	+X	2	If 2 has been disabled, use 9.
1-jet,-V	-X	9	If 9 has been disabled, use 2.

TABLE X

X-AXIS JET SELECTION POLICY

Type of translation	Normal policy	Alternate disabled-jet policy
4-jet,+X	2, 6, 10, 14	If either 2 or 10 has been disabled, use 6 or 14 If either 6 or 14 has been disabled, use 2 or 10.

TABLE X

X-AXIS JET SELECTION POLICY (cont)

Type of translation	Normal policy	Alternate disabled-jet policy
2-jet,+X (fuel system A)	2, 10	If either 2 or 10 has been disabled, use 6 or 14.
2-jet,+X (fuel system B)	6, 14	If either 6 or 14 has been disabled, use 2 or 10.
4-jet,-X	1, 5, 9, 13	If either 5 or 13 has been disabled, use 1 or 9. If either 1 or 9 has been disabled, use 5 or 13.
2-jet,-X (fuel system A)	5, 13	If either 5 or 13 has been disabled, use 1 or 9.
2-jet,-X (fuel system B)	1, 9	If either 1 or 9 has been disabled, use 5 or 13.

and acceleration. The control-law equations are basically a modification of a time-optimal solution, and are given as

$$K = 0.3M \ \frac{\frac{\Delta V}{\Delta t}}{I} \ L \ \dot{\delta} \tag{16}$$

$$\Delta = -\text{sgn} \left(K\dot{\theta} + \frac{\ddot{\theta}|\ddot{\theta}|}{2} \right) \tag{17}$$

$$u = -\text{sgn} \left[K^2\theta + \ddot{\theta} \left(\frac{\ddot{\theta}^2}{3} - \Delta K\dot{\theta} \right) + \Delta \left(\Delta K\dot{\theta} - \frac{\ddot{\theta}^2}{2} \right)^{3/2} \right] \tag{18}$$

The control output commands the sign of the change in angular acceleration. The sampling period for this mode is set at 200 milliseconds. Referring to Equation (16), the time-optimal law

is modified by a 0.3 gain factor in the assumed control-
effectiveness term K. This reduction is designed to avoid tran-
sient-response overshoot, and to prevent large steady-state limit
cycles. However, this gain should be kept reasonably high to
provide good transient-response characteristics.

The GTS control law associated with the acceleration-nulling
mode is designed to regulate the offset (disturbance) acceleration
from the descent thrust. The primary dynamical environments that
cause offset acceleration include shifting center-of-mass prop-
erties, DPS actuator compliance, and DPS engine-ablation effects.
This control law is structured in the form of a trim-gimbal drive-
time equation, and is given as

$$T = 0.4 \left| \frac{M \frac{\Delta V}{\Delta t} L \dot{\delta}}{I} \ddot{\theta} \right| \tag{19}$$

The principal sampling period associated with the acceleration-
nulling law is 2 seconds. However, under certain conditions, this
acceleration-nulling law is used as part of the basic RCS control-
law timing structure. The interaction and timing logic between
the RCS and GTS control laws are presented in the following
section.

RCS/GTS Interface

During DPS-powered flight, the GTS is generally adequate to
provide satisfactory control in the Q/R axes when the maneuver
requirements are slowly varying. It is believed that the GTS
should provide complete control (rather than regulation of the off-
set acceleration) whenever possible, to limit jet firings and to
minimize RCS propellant usage. During design of the DAP, a time-
shared control logic was developed in which the use of RCS and
GTS controls are interfaced to minimize mutual interaction.

The RCS/GTS interface has been designed so that the RCS
phase-plane state is examined for a logical decision (and the RCS
control law applied) at least every 200 milliseconds. The time-
line operation is as follows.

t	t + 100 msec	t + 200 msec	t + 300 msec
RCS control law	Test for (1) Attitude-control law (2) Acceleration-nulling law (3) RCS control law	RCS control law	Test for (1) Attitude-control law (2) Acceleration-nulling law (3) RCS control law

The test logic associated with use of the attitude-control law every 200 milliseconds is that the trim-gimbal drive times (in the Q- and R-axes) must be less than 2 seconds [Equation (19)], and that all U and V RCS jets must be off.

The requirements associated with the use of the acceleration-nulling law are that the attitude-control law must have been used on the previous pass, and that the test logic for present use of attitude-control law must have failed.

Therefore, in the RCS/GTS timing loop, the acceleration-nulling law is used only as a transaction between the attitude-control law and the RCS control law.

In addition to the RCS/GTS timing loop, another routine executes a test for the GTS acceleration-nulling law every 2 seconds. The nulling law is applied if, and only if, the trim gimbal is not under GTS attitude control (at least one of the two test conditions is not satisfied). This "captive" logic is designed to prevent a sustained thrust offset when the RCS control laws are commanding jet firings to counteract the disturbance acceleration.

HISTORY OF DESIGN DEVELOPMENT

The history of DAP development will be discussed by presenting base line designs for the design-formulation phase (September 1964 to December 1966) and for the SUNBURST flight-program phase (December 1966 to August 1967). Where applicable, comparisons will be made to the SUNDANCE base line design previously discussed. The significant problems encountered will also be discussed.

Apollo 5, the first (unmanned) LM mission, was launched into earth orbit January 22, 1968, and used the SUNBURST flight program. Following this mission, a decision was made to simplify the DAP logic, and a significant redesign of the control system was begun, resulting in the SUNDANCE digital program. This design version was flight tested on the first manned LM mission (Apollo 9), launched March 3, 1969. Subsequent lunar-landing missions will be flown using a slightly-modified SUNDANCE flight program.

Preliminary Design Development

Many modifications in design philosophy and in control-system implementation occurred during the preliminary design phase of DAP development. Excellent insight into the various control-system problems encountered is provided by reference 4. To establish background for a discussion of design problems, a base line

block diagram using assumed conditions was formulated (Figure 16).
The major design areas to be discussed include RCS control-law
formulation, estimation concepts, RCS/GTS control-mode interaction
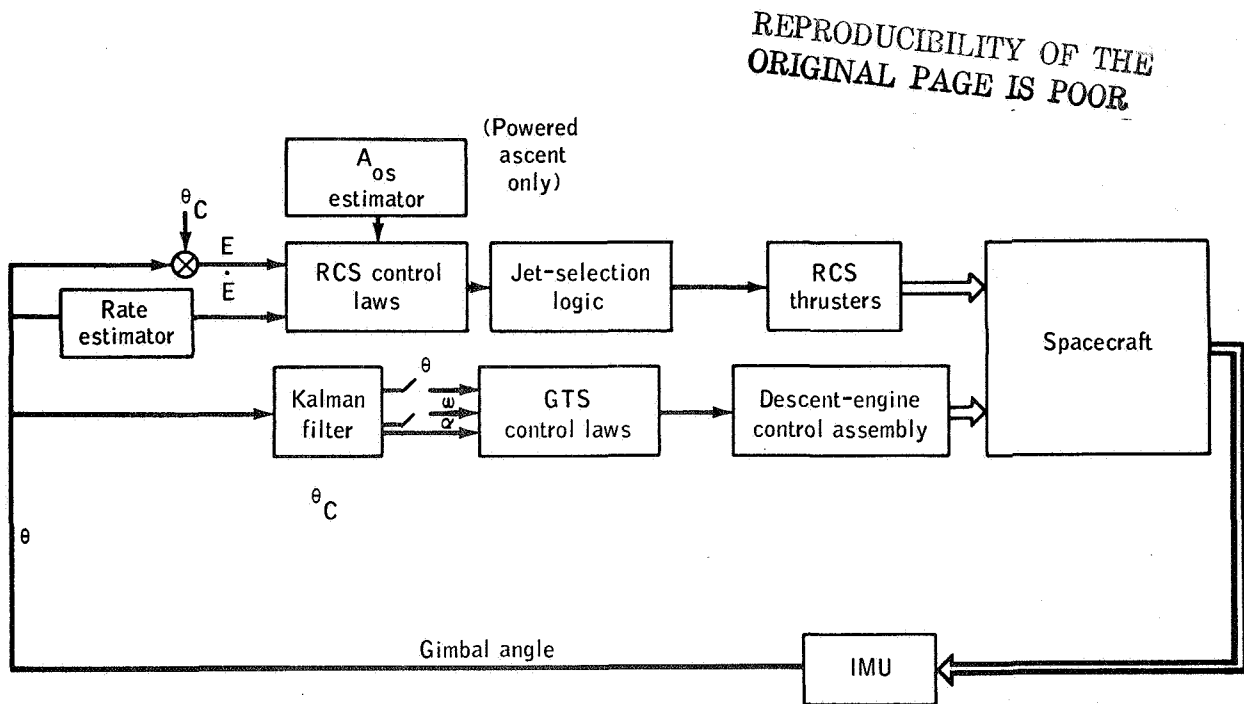logic, and RCS switching logic.

Figure 16. - Preliminary design control system

Three types of estimation programs were developed (an inte-
grated design concept had not established at that time). For
coasting flight, a simple rate estimator was established; for
powered ascent, a combined rate and acceleration estimator was
designed; and for powered descent, a Kalman filter was developed
for the GTS control-law function, and a rate estimator for the
RCS control-law function.

Two control modes were provided for the powered-descent
operation. The primary mode controls the Q- and R-axes with the
GTS, and the P-axis with the RCS. The secondary control mode
uses the RCS to control all rotational axes. The primary and
secondary control modes were designed to be exclusive as shown
by the interface logic (Figure 17). When any primary-logic con-
dition is exceeded, control is switched to the secondary mode,
and an open-loop GTS drive is performed, using data based upon

the drive time derived from Equation (19). A Kalman filter estimate of offset acceleration A_{os} is required, and is calculated in the primary mode in which undetected RCS jet failures are not a design factor. During the nominal secondary-mode operation, the RCS jets are commanded off every 10 seconds, and a Kalman filter estimate of the current offset acceleration is obtained. After this sequence, the RCS control is reinstated, accompanied by a new trim-gimbal open-loop drive. The logic conditions necessary to effect transfer from the secondary to the primary control are also presented in Figure 17. It should be noted that all conditions must be satisfied to return from secondary to primary control. The problems associated with this logic-design concept will be discussed in a following section.

Primary mode (GTS)	Primary mode (GTS)

I. Switch to secondary if
  1. E > 2 deg., or
  2. Ė > 0.65 deg./sec., or
  3. Change in throttle setting
II. Initiate open loop GTS drive
	Switch to primary if
	  1. E < 1.4 deg., and
	  2. Ė < 0.5 deg./sec., and
	  3. All jets are off

Secondary mode (RCS)	Secondary mode (RCS)
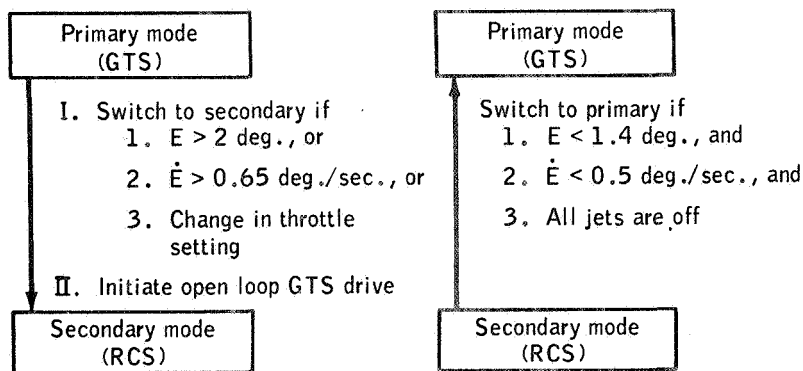
Figure 17. - Interface logic of the RCS/GTS

A significant design decision required in the initial developmental period was associated with the philosophy of RCS control law. The two fundamental concepts considered were a predictive control law based upon a two-point-boundary-value approach in the error phase plane, and a logic-determination technique requiring only present- and past-state information to calculate modulated jet commands. When the two concepts were being considered, the logic-modulation technique had the advantage of considerable design experience because of analog control-system development. Hence, the basic decision was whether to establish the control-law design by digitizing a known analog-autopilot concept, or by developing a predictive control law solely based upon digital principles.

The logic-determination techniques available included pulse-frequency modulation, pulse-width modulation, pulse-ratio modulation (PRM) delta modulation, and integral pulse-frequency modulation. The development of two proposed designs that use PRM techniques is discussed in references 5 and 6. The input to the

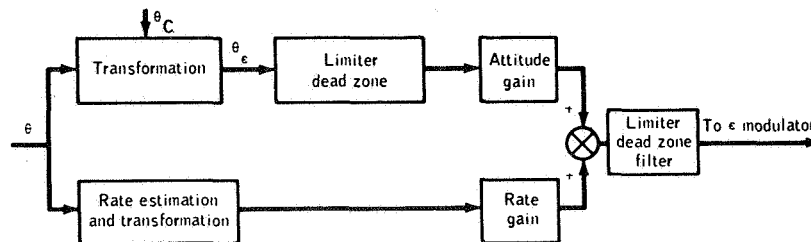modulator is typically obtained from attitude-error and rate information, as shown in Figure 18.

Figure 18. - Generation of control-error signal

The various trade-off factors between the digital PRM and the predictive control law are worthy of discussion. For nominal conditions, the predictive control law is generally more efficient in RCS propellant usage, (an I_{sp} penalty occurs for pulses shorter than 80 milliseconds), and usually commands a smaller number of jet firings. The principal disadvantages of the predictive approach include the sensitivity to plant uncertainties, such as inertia, thrust, and undetected jet failures, and the storage requirements for a large computer memory (parameter tracking, pre-diction logic, and recursive-filter techniques).

The most significant advantage of the digital PRM approach is that all logic is based upon present- and past-state infor-mation. Thus, for large off-nominal conditions, this approach has distinct advantages over the predictive design. The dis-advantages include the sensitivity to noise because of low-value threshold logic, and the large steady-state attitude offsets for sustained disturbance-torque conditions. The digital PRM system cited in reference 5 estimated a sampling-rate requirement of 30 to 40 samples per second. A modification to this PRM concept, in which both on-time and off-time were calculated and the sampling requirement was reduced to 10 samples per second, is discussed in reference 6. A general trade-off exists in the area of sampling, because a good predictive system will generally require lower sampling rates than a comparative logic-determination system. However, off-nominal environmental conditions (and basic plant un-certainties) tend to increase the sampling-rate requirements of a predictive system. Thus, an estimate of expected plant uncer-tainties and environmental conditions is important in establishing sampling-requirement trade-offs between predictive and logic-determination control laws. After extended consideration, the decision was made to develop a predictive control law for the DAP design.

The initial concept of the phase-plane switching logic is discussed in reference 7. This design concept includes a combination of parabolic and linear curves to represent the switching and targeting lines. The phase-plane logic, assuming a positive disturbance torque, is presented in Figure 19. The value of the intercept constant B is dependent upon the deadband, jet-control acceleration, and offset-disturbance acceleration. The basic purpose of establishing switching-line equations that vary with disturbance acceleration is to lower the average steady-state attitude error.

The phase-plane diagram contains the following labeled equations:

$$E = DB - \frac{\dot{E}^2}{2a_{netneg}}$$

$$E = -K\dot{E} - DB$$

$$E = -DB + \frac{\dot{E}^2}{2a_{netpos}}$$

$$E = -K\dot{E} + B$$

with axis markers $-DB$ and DB, and a legend indicating Coast region (hatched) and Thrust region (unhatched).
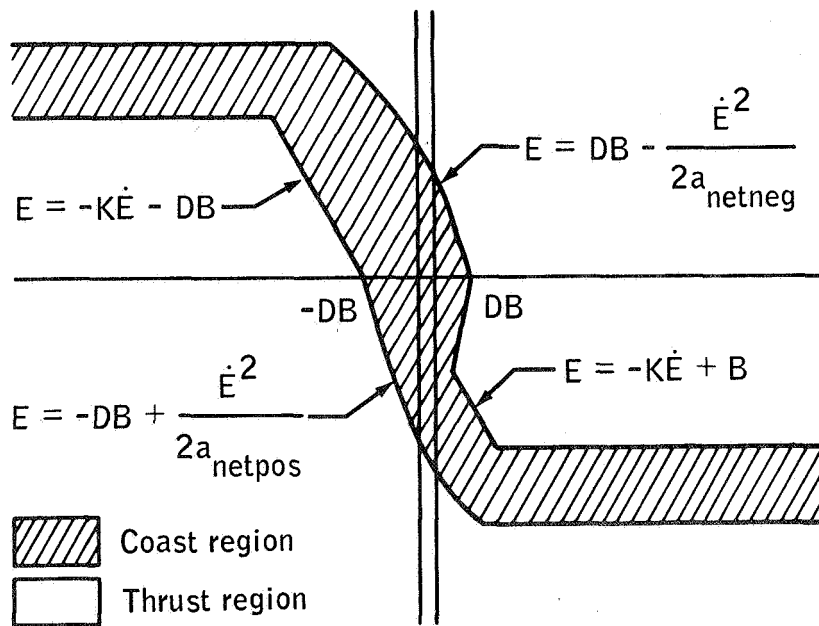
Figure 19. - Preliminary-design phase-plane logic

Most of the significant problems associated with the preliminary design were identified as a result of extensive simulation testing. The problem of estimating rate and acceleration when undetected jet failures existed proved to be especially difficult. Consideration was given to the use of multiple Kalman filters to estimate (from spacecraft dynamics) which of the 16 jets had failed, and to adjust the control functions accordingly. A second approach (subsequently implemented) was using the Kalman filter equations only when the GTS control law was operative or when the RCS jets were inhibited. However, disabling control during powered flight for the time needed to obtain good Kalman filter estimation was considered unacceptable and the technique was then discarded.

A second problem was that minimum-impulse operation was not achieved using the initial design. Design-verification studies indicated that this problem was caused by rate-estimation in-accuracies and quantization effects. Four phase-plane logic mod-ifications were considered: establishing a zone 3 concept (Figure 13), discounting the computed TJET time when in zone 2, setting the derived rate (under certain conditions) equal to a relatively large magnitude with the sign changed from the value used previously, and establishing the value FLAT as a function of inertia. The first modification was implemented in the prelim-inary design.

Significant design problems were identified with respect to Kalman filter performance. In simulation testing, this estimator was shown to be sensitive to slosh disturbances and large initial conditions. Furthermore, during the DPS start transient, the filter performance exhibited poor convergence because of engine compliance, propellant-fuel shift, and initial engine-mistrim conditions. The manner in which the Kalman filter estimate of acceleration was initialized was also of concern. The GTS open-loop drive technique influences how the initial acceleration estimate should be set for the next pass. The filter-extrapolation equations were also modified during the preliminary design phase. Originally„ the equations did not use information on the assumed GTS control effectiveness. The addition of the U_G term [Equation (10)] substantially improved the performance of the Kalman filter.

Another preliminary design problem concerned the vehicle performance during the DPS start transient. The convergence characteristics between the primary and secondary control modes were demonstrated to be marginal. The interaction of the GTS and RCS control modes under off-nominal conditions was of concern at that time, and proved to be a major motivation in the subsequent decision to redesign the control system.

The final problem concerned rate-overshoot performance during coasting maneuvers. The command-maneuver logic did not explicitly account for the finite time required to accelerate or decelerate to the desired maneuver rate, and additional jet firings resulted. To solve this problem, lag angles were provided to prevent over-shoot when initiating or terminating an automatic maneuver.

To conclude this section on preliminary design, a few general remarks on the control-system performance under off-nominal con-ditions are worthy of mention. Performance-verification studies indicated that the control system was insensitive to noise and small disturbance-torque conditions, but sensitive to inertia variations and thrust degradations (including undetected jet fail-ures).

SUNBURST Design Development

The base line design developed for the initial flight program (1) and design problems that occurred in that time period are presented in this section. The flight-test results of the SUNBURST DAP, flown on the Apollo 5 mission, will be presented in a later section. This description of the SUNBURST design emphasizes the modifications and additions to the preliminary base line design.

The state-estimator equations are structured in a manner similar to that outlined in the description of preliminary design. The rate equation for coasting flight is given by

$$\hat{\omega}_n = (1 - K) \left[\hat{\omega}_{n-1} + \alpha_J t_J \right] + \frac{K}{T} \left[\hat{\theta}_n - \hat{\theta}_{n-1} + \frac{\alpha_J t_J^2}{2} \right] \qquad (20)$$

The rate-estimation equation for powered flight is identical to Equation (20) except that the term $(1 - \frac{K}{2}) T \hat{A}_{os}$ is added to the right-hand side. $\hat{A}_{os}$ is defined as the estimated disturbance acceleration caused by a main-engine thrust. During descent, $\hat{A}_{os}$ is determined every control period (T = 0.1 second) by

$$\hat{A}_{os_n} = \hat{A}_{os_{n-1}} + \frac{M \frac{\Delta V}{\Delta t} L \dot{\delta}}{I} T \qquad (21)$$

For powered ascent, the A_{os} estimate is evaluated every 2 seconds by

$$\hat{A}_{os}\left(t_i\right) = C \, \hat{A}_{os}\left(t_i - 2\right) + \frac{(1 - C)}{2} \left[\hat{\omega}\left(t_i\right) \right.$$

$$\left. -\hat{\omega}\left(t_i - 2\right) - \int_{t_{i-2}}^{t_i} \alpha_j(t) \, dt \right] \qquad (22)$$

It is interesting to note that the rate- and acceleration-estimate equations are coupled for ascent. 'The filter gains, K and C, were established through detailed simulation testing. The nominal value of K for coast and descent is 0.5. The gains values

for ascent are time variant to accommodate a nominal offset-acceleration profile and are given as

$$K = 0.44 + \frac{0.56\,t}{400} \tag{23}$$

$$C = 0.25 + \frac{0.5\,t}{400} \tag{24}$$

Kalman filter equations are used during the primary (GTS) mode and are updated every 50 milliseconds. These equations are programed in gimbal-angle coordinates and are given as

$$\hat{CDU} = CDU' + W_0 \; \tilde{CDU} - CDU' \tag{25}$$

$$\hat{\dot{CDU}} = \dot{CDU}' + W_1 \; (\tilde{CDU} - CDU') \tag{26}$$

$$\hat{\ddot{CDU}} = \ddot{CDU}' + W_2 \; (\tilde{CDU} - CDU') \tag{27}$$

The assumed extrapolated state equations are expressed by

$$CDU'_n = \hat{CDU}_{n-1} + \hat{\dot{CDU}}_{n-1} T + \hat{\ddot{CDU}}_{n-1} \frac{T^2}{2} + U_G' \frac{T^3}{6} \tag{28}$$

$$\dot{CDU}'_n = \hat{\dot{CDU}}_{n-1} + \hat{\ddot{CDU}}_{n-1} T + U_G' \frac{T^2}{2} \tag{29}$$

$$\ddot{CDU}'_n = \hat{\ddot{CDU}}_{n-1} + U_G' T \tag{30}$$

where the assumed GTS control-effectiveness term is transformed to gimbal-angle coordinates.

A description of the RCS control laws associated with the SUNBURST design is necessary to the discussion of development. The basic structure of the switching lines was modified from the structure shown in Figure 19 to a format using only parabolic equations. Most of the design description has emphasized the single-plane aspects of the control-system development. A design area unique to the LM-thruster geometry (RCS jets 45 degrees from the body axes) was the logic of establishing the desired axes of rotation when simultaneous errors in pitch and roll occur. For the SUNBURST design, the Q/R axes were chosen for the control laws, and the concepts of urgency functions and urgency plane were established. Urgency functions in both the Q- and R-axes

were developed to measure the state location from the coast region, as well as to measure the RCS propellant penalty if the design to apply torque be deferred. These functions are approximately equivalent to the torquing time needed to reach the boundary of the coast region. The logic flow associated with the urgency-function concept is presented in Figure 20.

The urgency plane used to select the desired axis of rotation is illustrated in Figure 21.

The two urgency functions U_Q and U_R define a position in the urgency plane and thus establish the desired axis of rotation from the eight rotation sets available ($\pm R$, $\pm Q$, $\pm U$, $\pm V$). Additional logic is applied to determine the number of jets to be used in the chosen axis.

Two alternate approaches will give some insight into the design trade-offs. To illustrate the techniques, one must assume that the urgency functions in U_R and U_Q are initially established as shown in Figure 22a. The SUNBURST design logic will command a U rotation, then an R rotation, then a U rotation — until the urgency-function errors are nulled. An alternate design approach would be to null all U errors first, and then command the remaining R errors, as shown in Figure 22b.

The alternate approach is attractive in that advantage may be taken of the diagonal-jet moment arm; but, during certain disturbance-torque conditions, the delaying of the R correction could give undesirable performance. A second alternate approach (implemented in the subsequent redesign) would be to transform the original errors into the U- and V-axes, and to command U and V as shown in Figure 22c. Because the control-axis torques in U and V are decoupled, these corrections can be applied simultaneously. The logic simplifications that result from this design approach are significant; however, inefficiencies do occur for a detected jet failure, as discussed in reference 8.

A brief description of the GTS control laws associated with the SUNBURST design is needed. The time-optimal attitude-control law provided by equations (16), (17), and (18) was developed for the primary control mode in which the attitude-state errors are obtained from the Kalman filter equations. This design satisfies the requirement for an independently stabilized DPS control. The GTS acceleration-nulling law is used as part of the transfer logic from the primary mode to the secondary mode. The open-loop drive-time equation is

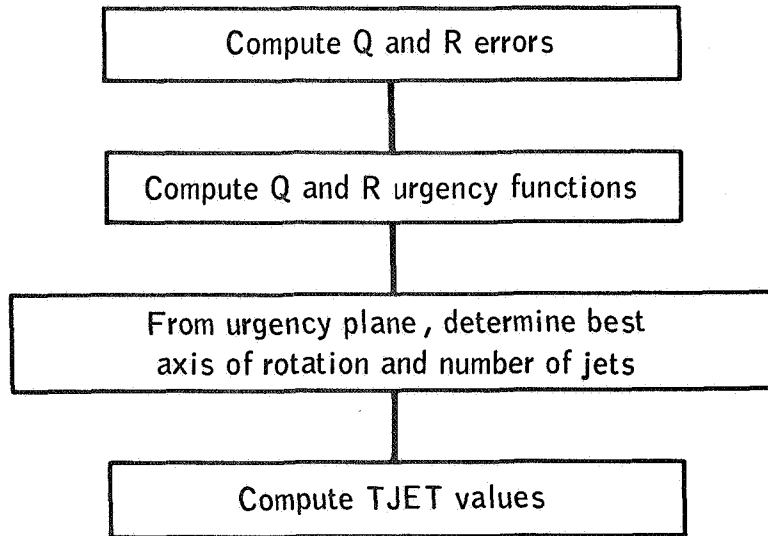$$T = \frac{\hat{\alpha}}{M \frac{\Delta V}{\Delta t} L \dot{\delta}} \qquad (31)$$

```
┌─────────────────────────────────────────┐
│       Compute Q and R errors            │
└─────────────────────────────────────────┘
                    │
┌─────────────────────────────────────────┐
│   Compute Q and R urgency functions     │
└─────────────────────────────────────────┘
                    │
┌─────────────────────────────────────────┐
│   From urgency plane, determine best    │
│   axis of rotation and number of jets   │
└─────────────────────────────────────────┘
                    │
┌─────────────────────────────────────────┐
│       Compute TJET values               │
└─────────────────────────────────────────┘
```

Figure 20. - Urgency-function logic flow
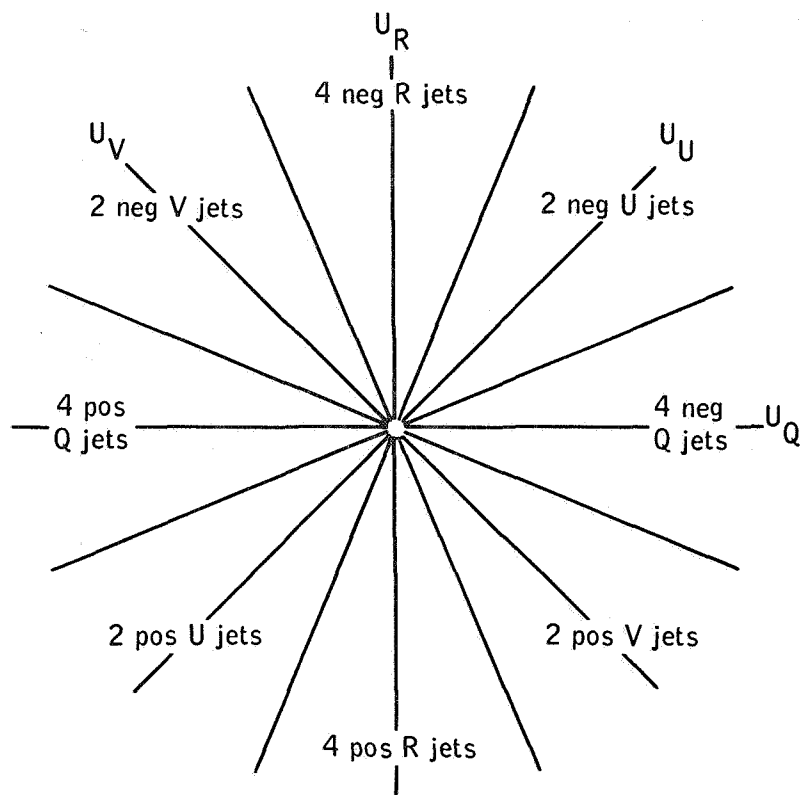
Figure 21. - Urgency plane
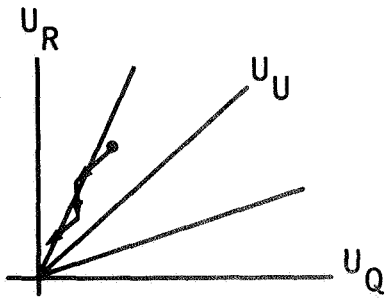
Figure 22a. - SUNBURST
urgency concept
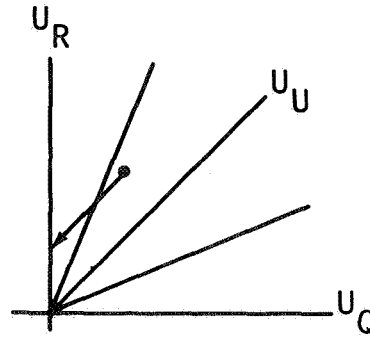
Figure 22b. - Alternate
SUNBURST urgency concept
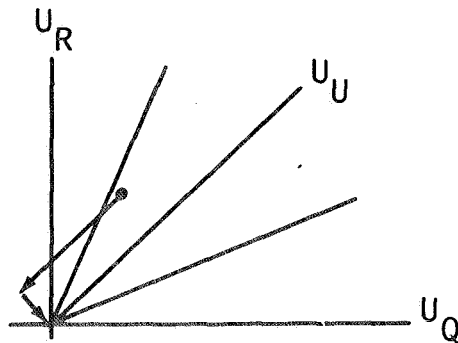
Figure 22c. - Another alternate SUNBURST urgency concept

where $\hat{\alpha}$ is the Kalman filter estimate of offset acceleration. A major difference between the SUNBURST design and the preliminary design was elimination of the technique of disabling RCS jets during powered flight to obtain Kalman filter estimation during the secondary control mode. This elimination restricted the GTS acceleration-nulling law function to an open-loop drive as part of the RCS/GTS transfer logic. The resultant performance problems associated with this interface will be discussed later.

The final SUNBURST design description to be presented are the Q- and R-axis jet-selection policies. The Q- and R-axis rotational policies for both normal and disabled-jet conditions, with alternate policies listed in order of preference, are presented in Table XI.

TABLE XI

Q- AND R-AXIS JET-SELECTION POLICIES

Type of rotation	Normal policy	Alternate disabled-jet policy
+Q	2, 5, 9, 14	2, 5; 9, 14; 2, 14; 5, 9
-Q	1, 6, 10, 13	1, 6; 10, 13; 1, 13; 6, 10
+R	1, 5, 10, 14	1, 14; 5, 10; 1, 5; 10, 14
-R	2, 6, 9, 13	6, 9; 2, 13; 2, 6; 9, 13
+U	5, 14	14; 5
-U	6, 13	6; 13
+V	1, 10	10; 1
-V	2, 9	2; 9
+Q (+X sense[a])	2, 5, 9, 14	2, 14; 2, 5; 9, 14; 5, 9
-Q (+X sense)	1, 6, 10, 13	6, 10; 1, 6; 10, 13; 1, 13
+R (+X sense)	1, 5, 10, 14	10, 14; 1, 14; 5, 10; 1, 5
-R (+X sense)	2, 6, 9, 13	2, 6; 6, 9; 2, 13; 9, 13

[a]The -X sense policies are only slight modifications of the +X sense policies listed.

Several problems occurred during the SUNBURST design phase. The general area associated with the descent primary/secondary mode interface was tested under extreme conditions, with particular emphasis upon the DPS start-transient performance. The nominal start-transient thrust profile for DPS powered-flight firings is presented in Figure 23. A "mass lockout" problem can occur for certain off-nominal conditions, when the thrust is operating at a maximum value of 10,500 pounds. One of the logic conditions needed for mandatory secondary control mode operation

is that a change in throttle setting has occurred. This logic is applied when a change in thrust command T_C is sufficiently large to satisfy the inequality.

$$T_C - M\frac{\Delta V}{\Delta t} > 525 \text{ pounds}$$

When T_C is operating at a maximum value of 10,500 pounds, a mass of 5 percent or more will cause the primary control mode to be locked out. The intent of this logic was to inhibit Kalman filter estimates of offset acceleration when actuator-compliance effects were introduced by changing throttling conditions. This potential problem with the interface logic was corrected in the SUNDANCE redesign.

The performance of the primary/secondary modes during the DPS start-transient period was of sufficient concern to require design modifications before the mission. The major problem was caused by errors introduced in the open-loop drive-time equation and by the subsequent poor convergence characteristics of the primary/secondary control modes. The effect of a drive-time error is to maintain a residual offset disturbance torque while the system is in the secondary mode. If this offset be large, the RCS jets converge the attitude and rate errors very slowly to the region in which return to the GTS control is made. During this period, the jets must fire to combat the sustained offset disturbance. An example of this type trajectory behavior is shown in Figure 24.

Factors that significantly contribute to the error in open-loop drive time are

1. Propellant-fuel shift during ullage and the low throttling-time period

2. Actuator mount compliance

3. Uncertainties in the assumed values of M, L, I, and $\dot{\delta}$

4. Kalman estimate of offset acceleration

    a. Insufficient measurements
    b. Propellant-slosh dynamics
    c. Attitude-rate initial conditions
    d. Measurement noise

Simulation testing indicated that these factors could seriously degrade the performance of the control system during the DPS start-transient period. Design modifications were made to improve the RCS/GTS logic interface and the quality of the Kalman estimate of offset acceleration. The modified interface logic is given in
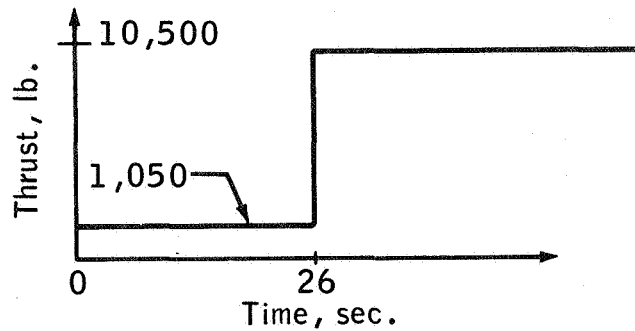
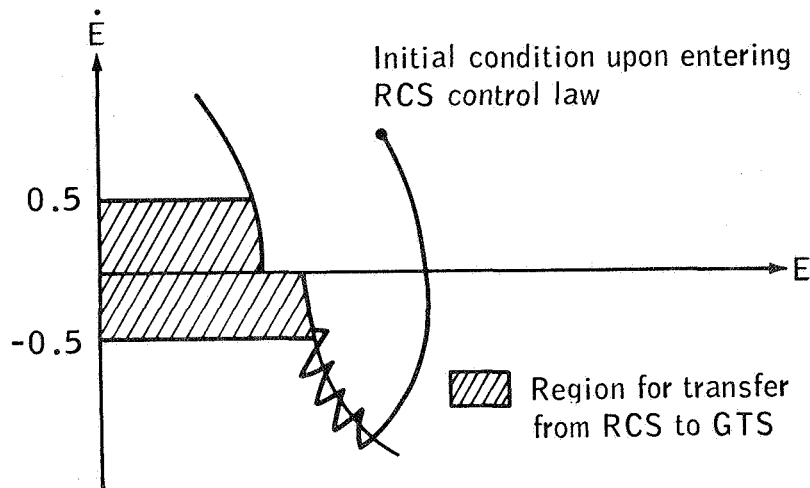Figure 23. - Throttle profile

Figure 24. - Example of RCS/GTS convergence

Figure 25. The interface logic shown provides significantly improved convergence characteristics at the expense of permitting large attitude errors during the transfer of control modes. The additional logic of insuring a minimum number of measurements for the Kalman filter was inserted because of the transient characteristic of the estimator. An actual acceleration-estimate response (9) is shown in Figure 26. For the simulation response shown, the acceleration estimate contained an error in sign for the first few measurements.

 Four additional design modifications were made to improve the DPS start-transient performance: modifying the Kalman filter weighting values, limiting the maximum open-loop drive time to 15 seconds, forcing the primary control (and Kalman filter estimates) at specific times when operating in the low-throttle re-
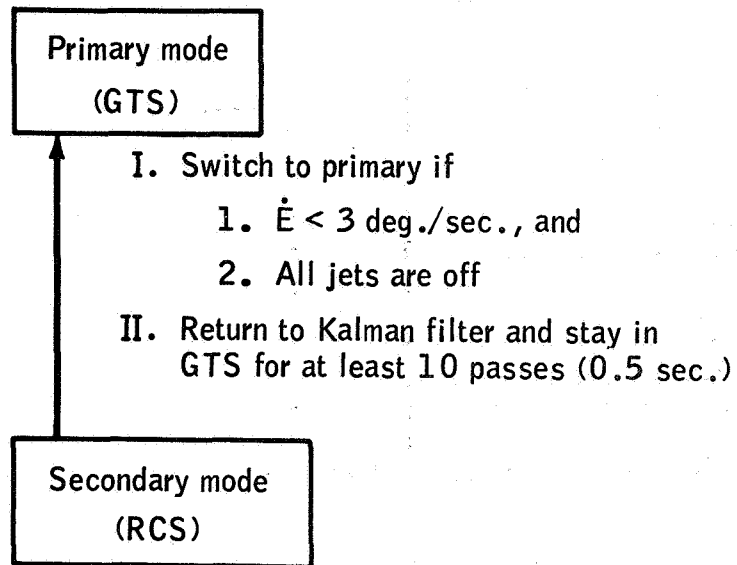
Figure 25. - Interface logic of RCS/GTS
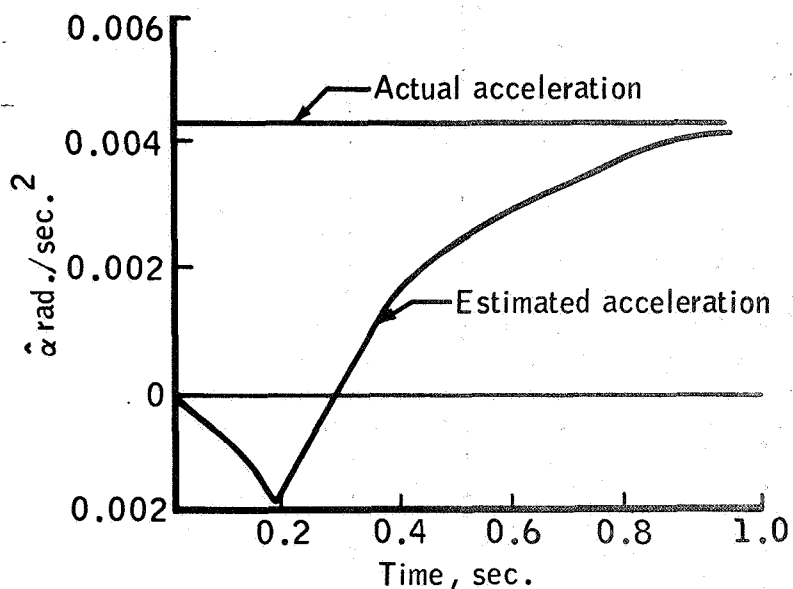
Figure 26. - Kalman filter transient performance

gion, and modifying the GTS attitude-control law during the 26-second start-transient period.

The modified GTS attitude-control law (for the start-transient period) is given by

$$u = -\text{sgn}(\hat{\alpha}) \tag{32}$$

The modified design was considered acceptable for the first un-
manned flight, although the inherent properties of the open-loop
gimbal drive was of concern.

In August 1967, a decision was made to redesign the DAP; the
SUNDANCE design, previously described, was the result of this re-
design effort. The objectives of the redesign were to reduce
memory-storage requirements, improve off-nominal performance, and
reduce computer-execution time. The five major changes that re-
sulted included elimination of the urgency-function concept,
simplification of the jet-selection logic, simplification of the
RCS control-law logic, improvement in the GTS/RCS interface de-
sign, and development of an integrated state-estimator design.

TESTING AND VERIFICATION

The mission-verification and design testing conducted on the
SUNDANCE DAP is discussed next. The primary objectives of pre-
flight testing were to validate the control-system performance
during nominal conditions, off-nominal conditions, and mission-
related conditions. The types of simulation facilities used in-
cluded engineering digital simulators, interpretive computer
simulators (ICS), and hybrid simulators.

Engineering simulators were used during initial development
(or modification) phases to provide dynamic validation and per-
formance evaluation of the functional design under a broad spec-
trum of mission conditions. The ICS bit-by-bit simulator modeled
the detailed computer characteristics, and was used to verify the
software-programing design. Parameter-type studies associated
with off-nominal performance are generally inefficient to run on
the ICS. However, nominal-performance verification is conducted
on a mission-by-mission basis. The hybrid simulators were used
to verify hardware/software interfaces, and to provide overall
system-performance validation. With respect to the DAP, both de-
sign-validation and mission-verification testing programs were
conducted on hybrid simulators.

The formal testing conducted on the SUNDANCE DAP design is
reported in references 8, 10, and 11. Reference 10 is an excellent
test-results document. All control modes of flight were tested
during nominal-performance conditions, RCS jet-failure conditions,
and incorrect-mass-property conditions. Powered-flight testing
included recovery from large rate and attitude errors, DPS/APS
start-transient performance, and performance with large offset
accelerations. A general summary of the test results follows.

1. Nominal performance was satisfactory (all modes).

2. Minimum-impulse limit cycles were achieved (coasting modes).

3. Efficient, automatic attitude maneuvers were achieved.

4. Translation-acceleration capability was degraded by jet failures.

5. Powered flight modes were relatively insensitive to inertia mismatch (errors of ±25 percent were tolerable).

Several test results from reference 10 are presented to indicate performance trends.

The RCS propellant consumed during a 2-degree-per-second maneuver is shown in Figure 27 as a function of mass mismatch. The theoretical fuel (1.21 pounds) is substantially below the
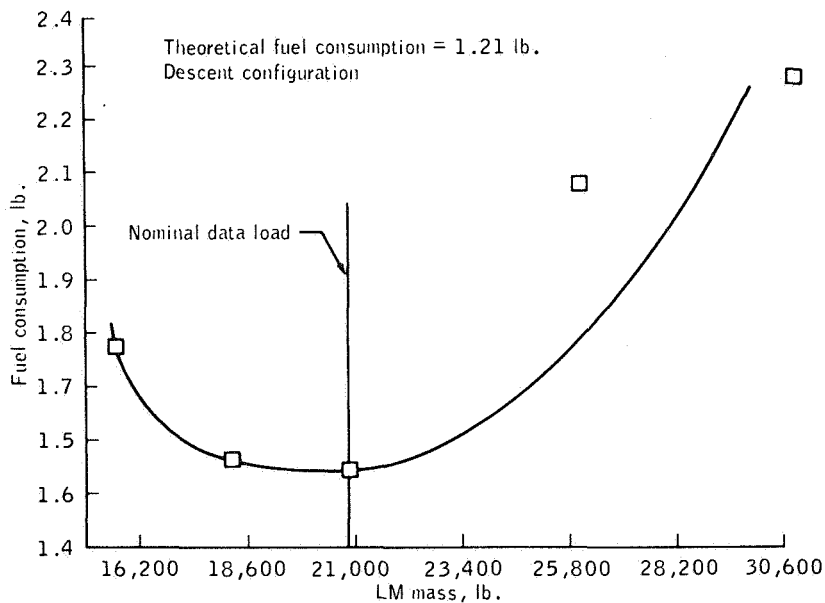
Figure 27. - RCS fuel for 2 deg /sec maneuver

minimum fuel usage (1.55 pounds), because the theoretical model does not account for jet-plume-impingement forces. A summary of descent-configuration maneuver performance for various jet-failed conditions is presented in Table XII.

For the third condition listed, the fuel consumed was less than nominal. The reason for this paradox is that the jet 10 im-

pingement force is larger than the impingement forces associated with the other jets, so that overall system efficiency is higher if jet 10 control be deleted.

The final performance curve shown is presented in Figure 28, in which the RCS propellant-versus-maneuver rate is presented for a LM descent configuration. The relative maneuver efficiency of the DAP design is difficult to assess because the theoretical fuel consumption used as a standard does not include the effects of jet plume impingement or the effects of crossproducts of inertia. The theoretical fuel consumption includes, however, the fuel required for acceleration and deceleration, the effect of crosscoupling torques, and the minimum-impulse fuel required to maintain the angular deadbands during the maneuver.

A brief summary of the hybrid-simulation test results re-ported in reference 8 will be given. The control system was sub-
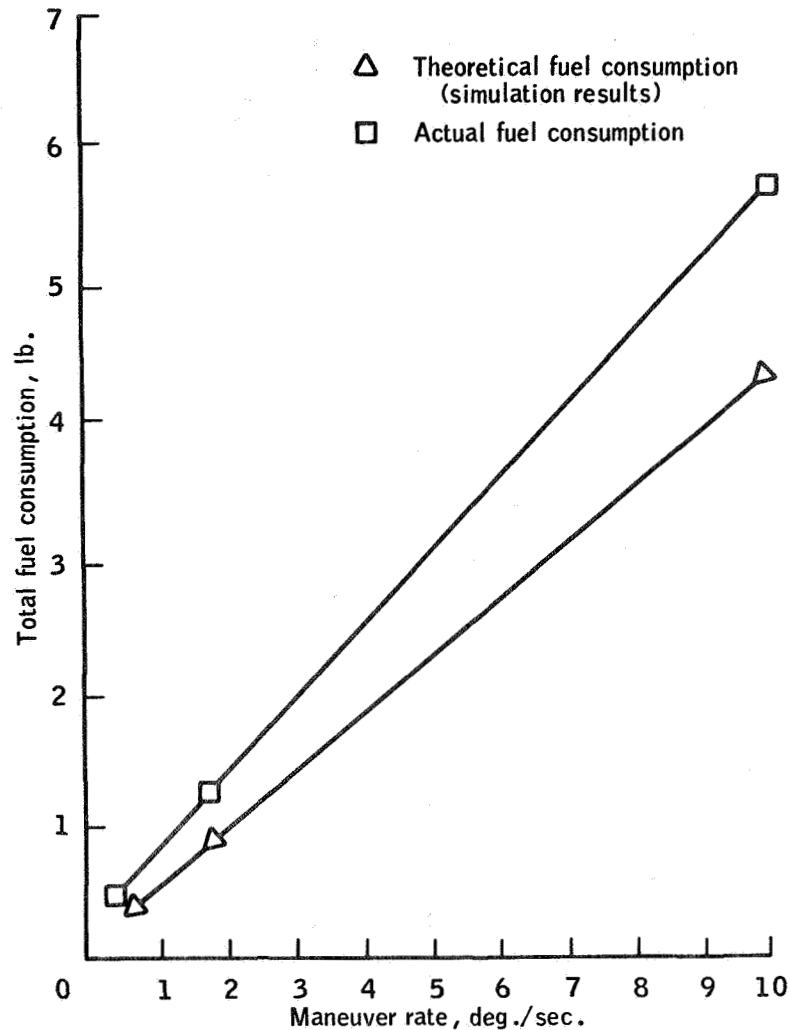
Figure 28.- Theoretical and actual RCS fuel comsumption for LM descent configuration

TABLE XII

DESCENT-CONFIGURATION MANEUVER TEST SUMMARY

Jets Failed	Maneuver rate, deg/sec		Maneuver		Fuel consumed during maneuver lb	Theoretical fuel needed to perform maneuver lb
	Desired	Greatest obtained	Desired gimbal angles	Gimbal angles at end of run		
None	2	2.04	20 80 40	19.01 81.09 39.25	1.55	1.21
Jets 10 and 11 failed off undetected	2	2.07	20 80 40	20.03 80.30 39.86	1.67	1.21
Jets 10 and 11 failed off detected	2	2.06	20 80 40	19.84 80.00 39.98	1.34	1.21
A system failed off undetected	2	2.09	20 80 40	19.48 80.86 39.47	1.83	1.21
A system failed off detected	2	2.03	20 80 40	20.17 80.00 40.48	1.55	1.21

jected to a realistic flight environment including the effects of RCS thruster impingement, propellant slosh, and actuator compliance. Off-nominal spacecraft environments included inertia, thrust, and center-of-mass uncertainties; DPS actuator-drive uncertainty; and RCS jet failures. The verification-run matrix associated with the hybrid testing was quite extensive. Integrated guidance and control hardware and a flight attitude table were used in the test facilities. Twenty-seven discrepancy items reported by the testing activity required formal disposition. Virtually all items requiring minor design modifications were incorporated into the lunar-landing-mission program.

An interesting design problem occurred in the area of inertia cross-coupling effects. With the TJET calculations established in the U/V-axes system, an RCS torque applied around the U-axis produces not only an acceleration around the desired U-axis, but also, in general, a coupled acceleration about the V-axis. The same situation applies to an RCS torque applied around the V-axis. The simplified equations of motion that demonstrate the effect of inertia crosscoupling are written as

$$\dot{\omega}_U = \frac{I_{yy} + I_{zz}}{2I_{yy} I_{zz}} M_U + \frac{I_{yy} - I_{zz}}{2I_{yy} I_{zz}} M_V \tag{33}$$

$$\dot{\omega}_V = \frac{I_{yy} - I_{zz}}{2I_{yy} I_{zz}} M_U + \frac{I_{yy} + I_{zz}}{2I_{yy} I_{zz}} M_V \tag{34}$$

where ω = angular velocity

M_U, M_V = applied torque

I_{yy}, I_{zz} = principal moments of inertia

This inertia crosscoupling effect between applied U/V torques and resulting U/V angular accelerations is significant only when the pitch and roll moments of inertia are substantially different. For powered-ascent operation, these inertia values were sufficient to cause crosscoupling that resulted in undesired limit-cycle performance. A subsequent design modification was made to eliminate the inertia crosscoupling effects. A nonorthogonal set of control axes U'/V' was defined which has the property that a pure U torque produces no observable acceleration in the V' direction, and a pure V torque produces no observable acceleration in the U' direction. This U'/V' nonorthogonal system can be constructed as shown in Figure 29.

The desired relationship between the U- and V-axes, and the U- and V-axes can be obtained if the transformation angle satisfies

$$\gamma = \cos^{-1} \frac{I_{yy}}{[I_{yy}^2 + I_{zz}]^{1/2}} - 45^{\circ} \tag{35}$$

The implementation of this control law where the crosscoupling accelerations are eliminated is described as follows. The vehicle state is estimated in the P-, Q-, R-axis system. When RCS control is to be applied, the Q and R components of error angle and rate are transformed to the U'/V' system. Errors about the U'-axis are controlled by firing a U-axis RCS torque, and errors about the V'-axis are controlled by firing a V-axis RCS torque.

FLIGHT TEST RESULTS

The flight results discussed include test data from the un-manned Apollo 5 mission and the manned Apollo 9 mission. Typical flight-data results are presented to indicate performance trends. The ability to match the preflight-simulation test results closely with the actual flight data is dependent upon the quality of the telemetered data and the knowledge of the spacecraft environment. In general, powered-flight maneuvers and coasting-flight attitude maneuvers can be closely duplicated, but attitude-hold limit-cycle behavior is more difficult to match in the postflight analysis process. For the test data shown, a data-sampling frequency of one sample per second was available.

Only the DAP coasting-flight modes were exercised on the Apollo 5 flight. Flight data for an automatic 5-degree-per-second attitude maneuver showed close agreement with simulation data. As reported in reference 12, the Apollo 5 mission provided some unplanned limit-cycle data during coasting ascent because of a mass-mismatch condition. This situation arose because, although the spacecraft was actually in an ascent configuration, the DAP computed the vehicle inertia to be that of the unstaged LM. As a consequence of the 300-percent inertia-mismatch condition, a virtually continuous-firing limit cycle resulted. The narrow-deadband attitude-hold logic did maintain the desired conditions, however. After this operation, one RCS propellant system was allowed to fire to depletion, and data were taken at various lower thrust levels as the propellant was being depleted. Almost immed-iately, the limit-cycle characteristics began to improve, and eventually the attitude-hold function settled into a minimum-impulse condition.

Limit-cycle data were also analyzed during the descent-coast phase of the Apollo 5 mission (13). Unexplained limit-cycle tra-

jectories in both pitch and roll phase planes, which were asymmetrical in computed error rate and symmetrical in attitude error, were observed. A representative trajectory is shown in Figure 30. During a 2-hour period, 125 jet firings occurred, approximately 30 of which had durations of from 50 to 110 milliseconds.

Preflight verification testing indicated that 16-millisecond (minimum-impulse) firings should occur at the deadband extremities. An extended effort was made to match the flight-test data through simulation testing. Inertia coupling, aerodynamic torques, and diagonal firing logic were all examined, but the observed limit-cycle phenomenon was only partially explained.

During another descent-coast phase, a different limit-cycle characteristic (Figure 31) was obtained. These trajectories contained 20-millisecond firing times, with the limit cycle restrained to one side of the attitude deadband.

This trajectory condition generally occurs during sustained torque disturbances. Limited post-flight data prevented identifying the exact nature of this disturbance, but a combination of aerodynamic torque and rate-estimation error was believed to have been the cause.

The Apollo 9 mission, during which the LM was manned for the first time, was flown in earth orbit. All powered- and coasting-flight DAP modes were exercised during the mission, and the control system performance was generally excellent. No anomalous or unexpected control-system conditions occurred. Data examined in the postflight analysis included peak-to-peak rates, attitude-deadband excursions, general limit-cycle characteristics (including existence of disturbance torques), and trim-gimbal performance.

Several flight-data results are given to indicate general performance. A 2-degree-per-second maneuver response for the ascent configuration is illustrated in Figure 32. A slight overshoot occurred in the Q- and R-axes, but overall rate performance was satisfactory. This overshoot was caused by rate-estimator errors.

A phase-plane plot of the limit-cycle performance during a powered ascent firing is presented in Figure 33. The intent of the plot is to trace the shape of the limit-cycle trajectory. Because of the data-sampling limitations, only discrete data points in the phase plane are available. The plot does indicate on a quantitative basis that the results are within a range consistent with preflight simulation results.
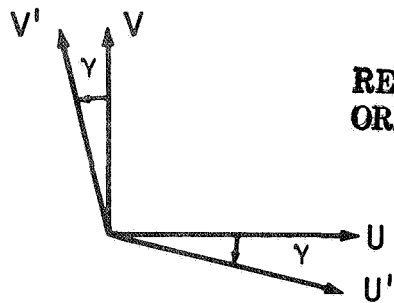
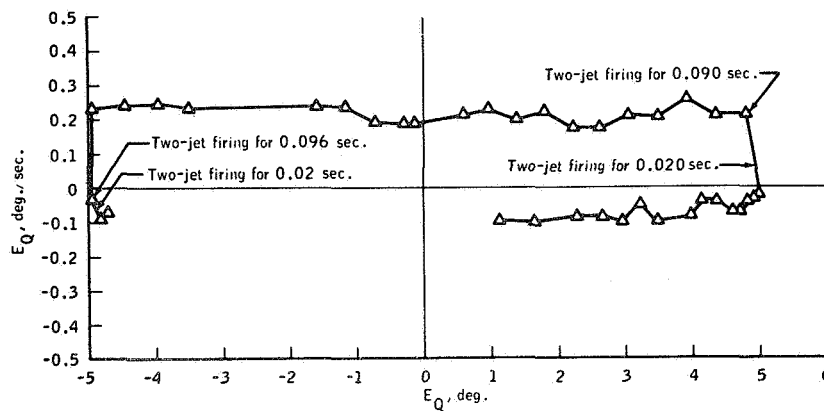Figure 29. - Nonorthogonal U'/V' system

Figure 30. - Pitch-rate error versus pitch error during
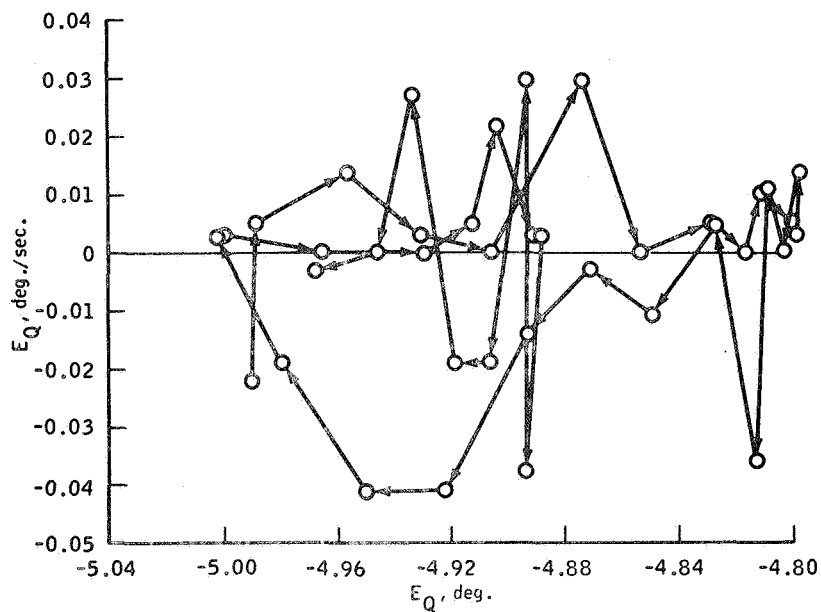a descent-coast phase

Figure 31.- Pitch-rate error versus pitch error during
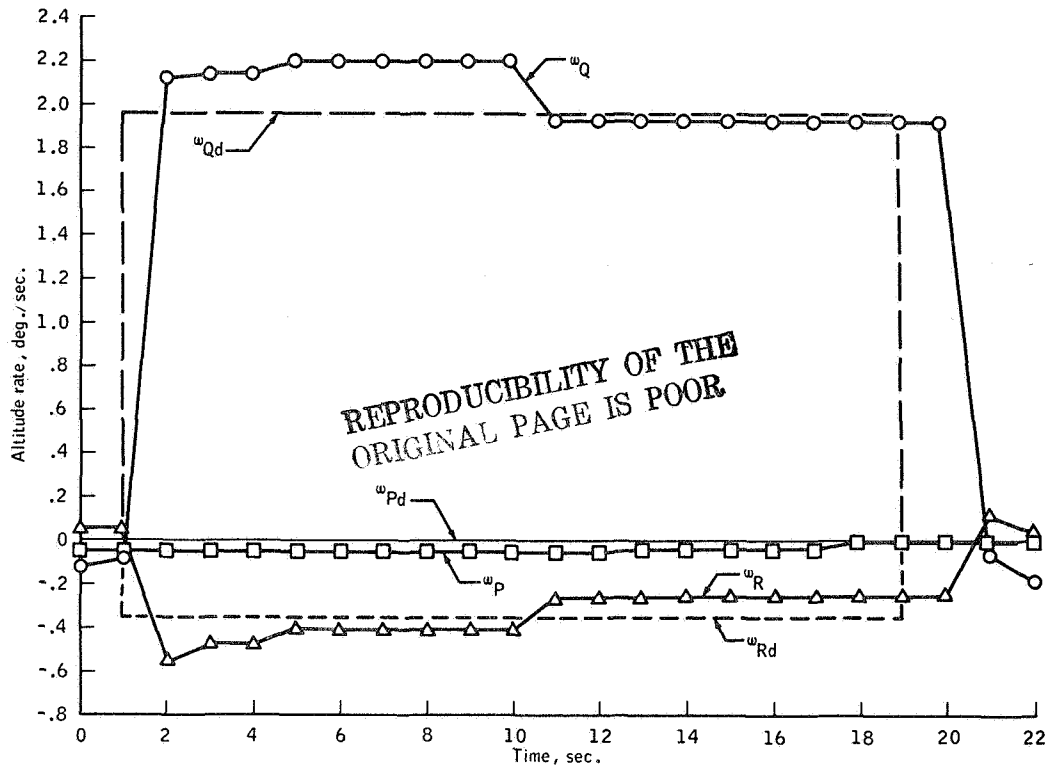another descent-coast phase

-58-

Figure 32. - Attitude maneuver during ascent-coast phase

The final Apollo 9 flight-test results presented (Figure 34) is a plot of phase-plane attitude performance during a DPS insertion firing. The results indicate nominal attitude-hold performance.

CONCLUSIONS

The history of the design and development of a first-generation digital control system has been presented in this case study. Because of the design flexibility inherent in digital systems, it is expected that increased emphasis will be placed upon digital control-system techniques.

This case study has been written to define the environment in which control-system designer works. Reviewing the design history, one gains an implicit perspective viewpoint of the relative importance of optimal control and modern control techniques.

Some of the experience learned during development of the DAP may be used to avoid future design problems. Logical decision techniques should be applied with care in the design development, because conditions may exist in which these techniques may un-
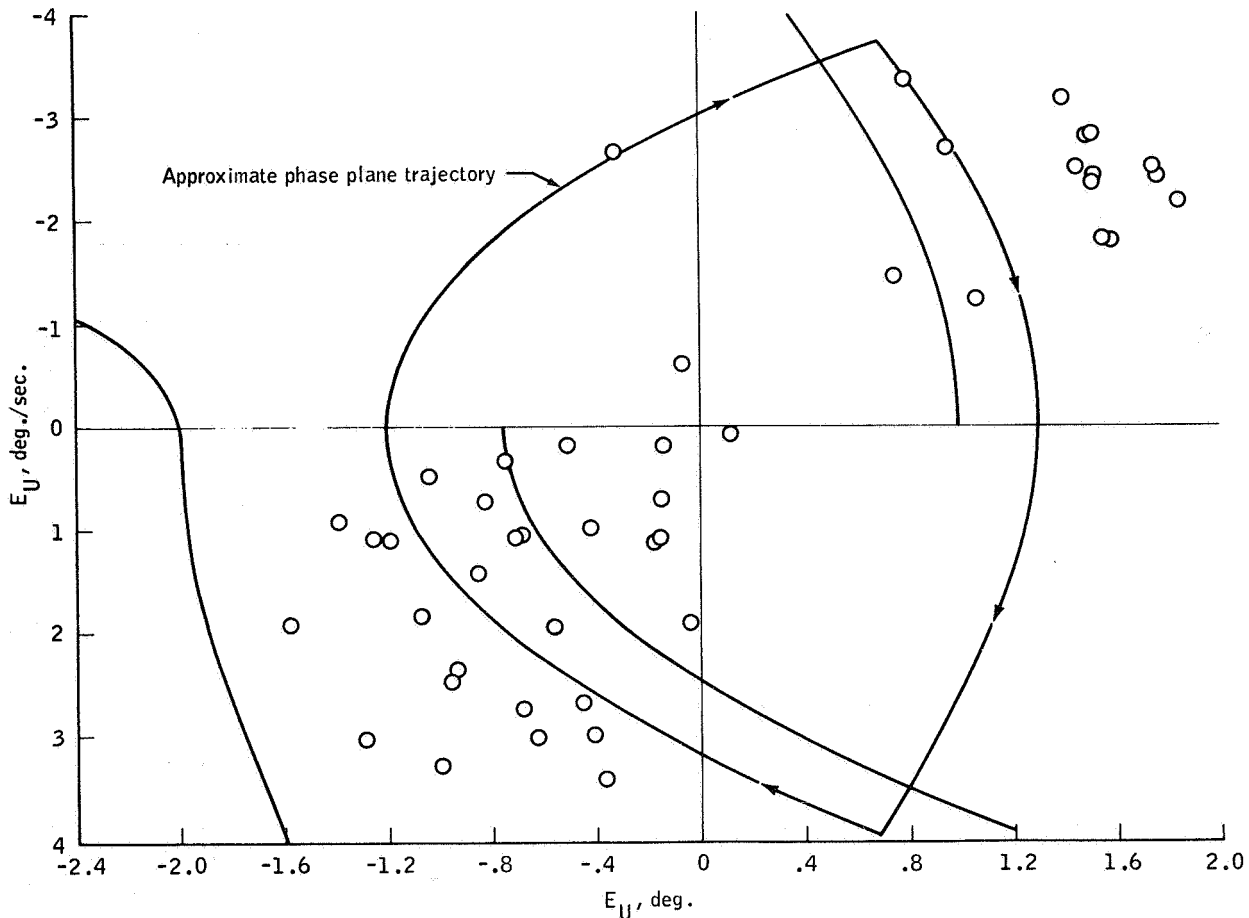
Figure 33. - Limit cycle during LM ascent firing

expectedly lock out entire system functions. The use of logic
in avoiding degraded performance has to be traded off with poten-
tial unintended restrictions.

Another generalization concerns the manner in which require-
ments in the estimation function are established. Open-loop
testing alone is not always adequate to assess the acceptability
of the filter performance. Estimation requirements should reflect
the manner in which the output information is used in the control
law. As an example, a control law that is mechanized to operate
on the sign of a function only has different requirements from a
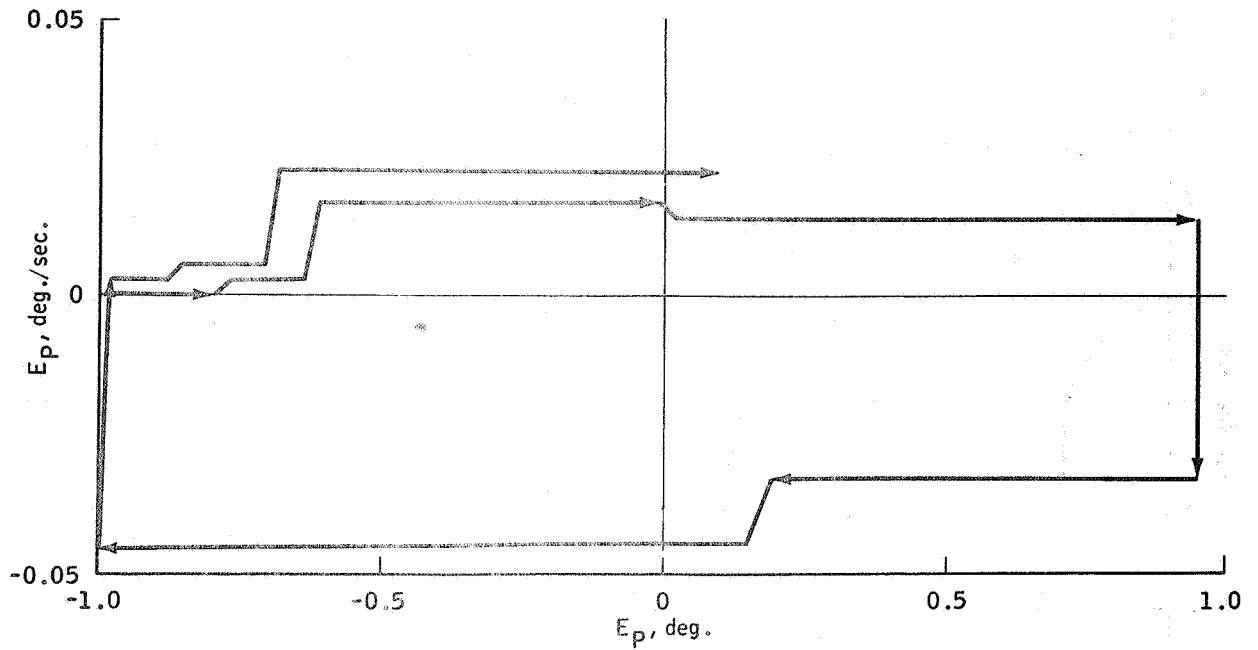law that operates on both sign and magnitude.

Figure 34. - Limit cycle during LM descent firing

Further research effort should be expended to develop additional analytical techniques for digital control-system design. Adaptive design techniques making use of the inherent flexibility available in digital systems should also be established.

REFERENCES

1. "Guidance System Operations Plan AS-206," MIT Instr. Lab.,
    Rep. R-527, Vol. I, Rev. 1 (Jan. 1967)

2. Covey, R. R., R. B. Sherwood, and S. H. Wu, "Apollo Digital
    Reaction Control System Design Studies," TRW Space Technology
    Lab., Rep. 4181-6010-KU000 (Apr. 5, 1965)

3. "Guidance System Operations Plan for Manned LM Earth Orbital
    Missions Using Program SUNDANCE," MIT Instr. Lab., Rep. R-557,
    Sec. 3 (Sept. 1968)

4. "Design Verification and Performance Evaluation of the Lunar
    Module Digital Autopilot," TRW Systems Group, Rep. 05952-
    6078-R0-00 (Nov. 1966)

5. "Preliminary Analysis of Sampling Rate Requirements and
    Digital Computer Functional Considerations for Design of LEM
    Digital Autopilot," GAEC, Rep. LM0-500-211 (Sept. 9, 1964)

6. Heiber, A., J. M. Nervik, and E. A. Nussbaumer, "Apollo Block
    II CM and LM Guidance and Control Study," Bellcomm, Inc.,
    TM-64-1021-3 (Dec. 17, 1964)

7. Cherry, George, and Joseph O'Connor, "Design Principles of
    the Lnnar Excursion Module Digital Autopilot," MIT Instr.
    Lab., Rep. R-499 (July 1965)

8. "Performance and Analysis of GFE SUNDANCE Digital Autopilot,"
    GAEC, Rep. LED-500-23 (Feb. 1969)

9. "Evaluation and Analyses of GFE Digital Autopilot (DAP) Per-
    formance," GAEC, Rep. LED-500-17 (July 1967)

10. "LM Digital Autopilot Simulation Results Using Program
    SUNDANCE," MIT Instr. Lab., Rep. E-2377 (Jan. 1969)

11. "Digital Autopilot Software Verification Test Results Summary
    for Mission D - SUNDANCE and COLOSSUS IA," TRW Space Tech-
    nology Lab., Rep. 11176-H149-R0-00 (Feb. 1969)

12. "LM-1 Guidance and Control Systems Postflight Analysis,"
    GAEC, Rep. LM0-500-657 (Apr. 5, 1968)

13. "Supplement 4 to Apollo 5 Mission Report - Analysis of Digital
    Autopilot Performance," TRW Space Technology Lab., Rep.
    11176-H061-R0-00 (Oct. 1968). Also available as MSC-PA-R-
    68-7, Supplement 4 (Jan. 1969)